INVESTIGATING THE EFFECTS OF PERCEPTUAL LEARNING ON THE FUNCTION AND MICROSTRUCTURE OF THE VISUAL CORTEX

A THESIS SUBMITTED TO

THE GRADUATE SCHOOL OF ENGINEERING AND SCIENCE

OF BILKENT UNIVERSITY

IN PARTIAL FULFILLMENT OF THE REQUIREMENTS FOR

THE DEGREE OF

MASTER OF SCIENCE

IN

NEUROSCIENCE

By

Dilara Erişen

December 2020

Investigating the effects of perceptual learning on the function and microstructure of the visual cortex
By Dilara Erişen
December 2020

We certify that we have read this thesis and that in our opinion it is fully adequate, in scope and in quality, as a thesis for the degree of Master of Science.

Hüseyin Boyacı(Advisor)

Burcu Ayşen Ürgen

Dicle Nahide Dövencioğlu

Approved for the Graduate School of Engineering and Science:

Ezhan Karaşan
Director of the Graduate School

ABSTRACT

INVESTIGATING THE EFFECTS OF PERCEPTUAL LEARNING ON THE FUNCTION AND MICROSTRUCTURE OF THE VISUAL CORTEX

Dilara Erişen
M.S. in Neuroscience
Advisor: Hüseyin Boyacı
December 2020

Perceptual learning is the long-term improvement of the ability to process sensory stimuli through experience. Although an extensively studied field, the mechanism and locus of plasticity underlying visual perceptual learning is subject of debate. Here, we investigated the experience-dependent plasticity in the visual cortex across the time course of perceptual learning of bisection discrimination task. Population receptive field (pRF) analysis was used to examine functional architecture of the visual cortex. Microstructural properties of the visual cortex were characterized with neurite orientation dispersion and density imaging (NODDI). We compared pre-, mid-, and post-training values of pRF size, neurite density, and orientation dispersion in the trained location as well as in two control locations where no training has been received. The values in the trained location did not change with time and did not differ from control locations. In addition, we assessed the microstructural properties in the white matter tract between the training location and the mirror-symmetric control location and did not observe any change with training. In conclusion, we found no training-related changes in the early visual cortex (V1-V3). Our results are limited by the lack of performance improvement with training and the small sample size. Moreover, we were not able to identify visual areas beyond V1-V3 leaving high-level visual areas unexplored. Suggestions for further research include redesigning the behavioral training paradigm, optimization of pRF protocol to identify high-level visual areas, and repeating the study with a larger sample size.

Keywords: visual perceptual learning, bisection discrimination task, population receptive field analysis, noddi, experience-dependent neuroplasticity.

ÖZET

ALGISAL ÖĞRENMENİN GÖRSEL KORTEKSİN İŞLEVİ VE MİKRO YAPISI ÜZERİNDEKİ ETKİLERİNİN ARAŞTIRILMASI

Dilara Erişen
Nörobilimler, Yüksek Lisans
Tez Danışmanı: Hüseyin Boyacı
Aralık 2020

Algısal öğrenme duyusal uyaran işleme yeteneğinde deneyim ile meydana gelen uzun vadeli gelişmedir. Kapsamlı olarak çalışılmış bir alan olmasına rağmen, görsel algısal öğrenmenin altında yatan plastisitenin mekanizması ve yeri halen tartışma konusudur. Bu çalışmada, iki parça ayırma görevinin algısal öğrenme süreci boyunca görsel kortekste deneyime bağlı plastisiteyi araştırdık. Görsel korteksin fonksiyonel yapısını incelemek için popülasyon alıcı alan analizini kullandık. Görsel korteksin mikroyapısal özelliklerini, nörit oryantasyon dispersiyonu ve yoğunluk görüntüleme (NODDI) ile karakterize ettik. Eğitim lokasyonun yanı sıra eğitim alınmayan iki kontrol lokasyonunda popülasyon alıcı alan boyutu, nörit yoğunluğu ve oryantasyon dağılımının eğitim öncesi, eğitim sırası ve eğitim sonrası değerlerini karşılaştırdık. Eğitim konumundaki değerler zamanla değişmedi ve kontrol konumlarındaki değerler ile farklılık göstermedi. Buna ek olarak, eğitim yeri ile ayna simetrik kontrol konumu arasındaki beyaz cevher yolundaki mikroyapısal özellikleri değerlendirdik ve eğitimle herhangi bir değişiklik gözlemlemedik. Sonuç olarak, erken görsel kortekste (V1-V3) eğitimle ilgili bir değişiklik bulmadık. Sonuçlarımız eğitimde performans artışı olmayışı ve küçük örneklem boyutu nedeniyle kısıtlıdır. Ayrıca, V1-V3'ün ötesindeki görsel alanları belirleyemediğimiz için ileri seviye görsel alanlar araştırılamamıştır. Gelecek araştırmalar için davranışsal eğitim paradigmasının yeniden tasarlanması, popülasyon alıcı alan protokolünün ileri seviye görsel alanları belirleyecek şekilde optimizasyonu ve çalışmanın daha büyük bir örneklem büyüklüğüyle tekrarlanması önerilir.

Anahtar sözcükler: görsel algısal öğrenme, iki parça ayırma görevi, popülasyon alıcı alan analizi, noddi, deneyime bağlı nöroplastisite.

Acknowledgement

First of all, I would like to thank my advisor Hüseyin Boyacı for his academic guidance during my master's studies as well as the kind encouragement and the meticulous feedback he provided in the writing of this thesis. I would like to thank Erhan Genç for sharing his expertise and mentoring me through every step of my research. I very much appreciate the generous help Benjamin de Haas provided in establishig our pRF protocol. I would like to express my appreciation to my committee members Burcu Ayşen Ürgen and Dicle Dövencioğlu for their insightful comments and helpful suggestions to forge this work into its final shape.

I am sincerely grateful to my collaborator Beyza Akkoyunlu. We certainly had our fair share of misadventures while working on this project but still made a good team. I could not ask for a better company while sitting through MRI sessions that felt like an eternity and stress-eating entire jars of peanut butter. I had great pleasure of working with Batuhan Erkat who made the time to answer every little question I had on pRF analysis and never made me feel bad even when I asked the same question for the third time. I would like to thank Cemre Yılmaz for sharing her insights on pRF analysis; Rabia Şen for taking the time to read my thesis; and Ecem Altan for finding ways to support my research from another hemisphere.

I would also like to extend my gratitude to Buse Merve Ürgen for letting me learn from her experiences and patiently advising me on my self-fabricated personal dilemmas. I would like to thank Sertaç Üstün who offered his sympathetic ear whenever I have needed to vent and reassured me that I am not alone in my troubles. I am also thankful to Emre Kale for taking me on as his padawan before I have started my studies at Bilkent University.

My deepest gratitude to my great friends that I am too lazy to name one by one. They somehow managed to be always there for me whether we were separated by schedules, time zones, or lockdowns. I am truly thankful to my parents Serpil and Ahmet. Their consistent confidence in me fueled my own and

helped me through many moments of doubt. Lastly, I would like to thank my feline friend Matilda for her warm and playful companionship.

Contents

List of Figures

List of Tables

Chapter 1

Introduction

Perceptual learning is the long-term performance improvement in a sensory task through repeated practice. The trained individual develops the ability to quickly detect and reliably identify the sensory attributes that are indistinguishable to the untrained individual. This kind of ability is particularly remarkable in real-life perceptual experts such as radiologists, wine tasters, and chicken sexers. Perceptual learning is often considered to arise from experience-dependent neuroplasticity making it a popular research topic in neuroscience. However, the mechanism and locus of plasticity underlying perceptual learning are still undetermined.

The work reported in this thesis aims to investigate the experience-dependent plasticity in the visual cortex over the course of perceptual learning of a visual task. For this purpose, magnetic resonance imaging (MRI) data were collected at different time points during training with bisection discrimination task. Population receptive field analysis was used to assess changes to the functional architecture of the visual cortex. Structural changes to white and gray matter were studied with diffusion weighted imaging.

This introduction provides an overview of the prominent conceptual frameworks guiding visual perceptual learning (VPL) research and reviews the literature with a special focus on neuroimaging findings. It then presents the scope and motivation of the present study.

1.1 Visual Perceptual Learning

Early psychophysical research of VPL showed that performance improvement is specific to some visual features such as the trained eye, retinal location, orientation, and spatial frequency. The specificity of improvement was interpreted as implicating the primary visual cortex (V1) as the locus of learning. V1 contains monocular cells that respond to stimulation of only one eye. Consistent with high location specificity of learning, receptive fields in primary visual cortex are smaller compared to other visual areas. In addition to stimulus position, V1 neurons show selectivity to stimulus attributes including orientation and spatial frequency. Based on the compatibility between observed learning specificities and known characteristics of V1, VPL was regarded as a manifestation of adult V1 plasticity [1]. A new insight into the visual cortex was thus provided, according to which experience-dependent plasticity is retained to some degree in adulthood in contrast to the prevalent notion of a critical period for neuroplasticity [2]. The specificity of learning and the inferred role of V1 plasticity have since been a major focus of VPL research.

Later research created a discrepancy regarding the specificity of VPL as some transfer of learning to untrained stimulus locations and features were reported. This gave rise to new theories of the neural basis of VPL favoring more generalized mechanisms. For example, the reverse hierarchy theory asserts that learning starts at high-level visual areas where the neurons have larger receptive fields and respond to broader range of stimulus attributes [3, 4]. Thus, practice-induced plasticity at high-level visual areas underpins the generalized performance improvement in the earlier stages of VPL. However, fine-grained spatial discrimination provided by lower-level visual areas is required as the training proceeds and

the task difficultly increases. At these later stages, plasticity reaches to lower-levels by top-down cascades and performance improvement becomes spatially specific.

Another alternative view is the selective reweighting model of perceptual learning. In this model, learning occurs in the connections from early visual representations to the decision system [5, 6]. This decision system can be understood as the higher-level visual areas that receive input from early ones. In contrast to the primary visual cortical plasticity theory and the reverse hierarchy theory, sensory representations remain stable in the selective reweighting model. The performance improvement arises from improved readout or decoding of sensory information from task-relevant sensory representations. This model predicts failed transfer of learning to an untrained condition when the sensory representation, the decision system or both are distinct between trained and untrained conditions.

A major finding in the psychophysical research of VPL has been the complete transfer of performance improvement to another location where additional training with an irrelevant task was received [7]. For example, when participants were trained with contrast discrimination task at one location and orientation discrimination tasks at a second location, the increased ability to discriminate contrast was transferred to the second location. The elimination of location specificity with the double-training paradigm further challenges the primary visual cortical plasticity theory and supports the involvement of higher-level visual areas. Nevertheless, it is difficult to identify neural mechanisms that underlie VPL solely by means of psychophysics.

Neurophysiological investigation of VPL studies the changes in receptive field properties of neurons such as location, size, and stimulus feature selectivity. The stimulus feature is encoded with the response profile of the neuron. The spiking activity of a neuron forms a bell-shaped curve when plotted as a function of the stimulus feature. The stimulus configuration the neuron is most sensitive to elicits the highest response and constitutes the peak of the curve. This so-called neuronal tuning curve is a standard method in neurophysiological research

to characterize the response profile of a neuron. The slopes of the orientation tuning curves of V1 neurons responding preferentially to trained stimulus orientation were shown to increase in monkeys trained with orientation discrimination task [8]. The sharpening of neuronal tuning was interpreted as the increased discriminatory ability of the trained neurons. Another group reported no changes in the tuning characteristics of trained neurons in monkey V1 and V2 using similar training [9] whereas sharper orientation tuning curves were observed in V4 [10]. When cats were trained on an orientation discrimination task using near-threshold low contrast gratings, contrast sensitivity in V1 neurons most sensitive to the trained spatial frequency was found to increase[11].

There are also neurophysiological findings indicating the involvement of areas beyond visual cortex in VPL. Receptive field properties in monkey V1 were not changed following training with bisection discrimination task [12]. However, response profile of V1 neurons were modulated by stimuli placed outside the receptive field. The modulation was stronger during task performance. This contextual influence was suggested to result from modulation of horizontal connections between neurons via feedback from higher cortical areas. The top-down modulation in V1 was further investigated in another study with monkeys trained to perform two different tasks (Vernier and bisection discrimination) using the same five-line stimulus presented at the same visual location[13]. It was shown that the neuronal responses in V1 were selectively modulated by behaviorally relevant attributes of the stimulus. Performance improvement in motion discrimination task was found to correlate with changes in the response properties of neurons in the lateral intraparietal area (LIP) but not in the middle temporal area (MT) [14]. The change in LIP responses was interpreted as more selective readout of the sensory representation in motion-sensitive visual area MT.

Neural correlates of VPL in humans were explored predominantly using functional MRI (fMRI). Following one day of monocular training in texture discrimination task, increased activity in V1 was observed when the stimulus was presented to the trained eye as compared to the untrained eye. Furthermore, functional connectivity analysis revealed greater coupling between V1 and several areas beyond visual cortex during the untrained condition suggesting that the

initial task performance is mediated by higher cognitive processes [15]. Increase in V1 activity was also reported after one month of training with orientation discrimination task [16]. Two possible neural mechanisms were suggested: increased spiking rates in neurons most sensitive to the the stimulus orientation or an increase in the number of neurons responding to the stimulus. Another study examined the changes in activation in visual cortex for an extended time course of training using texture discrimination task [17]. Consistent with the previous reports, V1 activation was found to increase at the beginning. However, after a few sessions of training the activation in V1 returned to baseline level, coinciding with the performance saturation. An initial increase in synaptic connections followed by synaptic downscaling was suggested as the mechanism of observed activation changes.

Although fMRI is a powerful tool for non-invasive whole-brain investigation, conventional analysis methods provide limited information about brain mechanisms underlying observed activation changes. An alternative framework is computational fMRI which exploits machine learning algorithms and/or theory-driven computational models in order to provide more mechanistically meaningful insights into brain-behavior relationship. Unlike conventional fMRI which focuses on localizing the task-related cortical areas, computational fMRI aims to identify the computational role of a brain area. The analysis approaches include investigating distributed patterns of neural representations by multivariate analysis, volitional control of neural activity by real-time fMRI analysis and predicting hypothetical signals associated with the behavior by model-based analysis [18]. Recent neuroimaging studies of VPL benefit from these more advanced analysis methods.

The use of computational fMRI in VPL research has revealed mixed evidence. VPL of an orientation discrimination task was investigated by combining reinforcement learning model and multivariate decoding analysis [19]. Stimulus orientation was shown to be encoded in early visual areas as well as higher cortical areas such as LIP and anterior cingulate cortex (ACC). However, behavioral improvements in the orientation discrimination task correlated only with changes in ACC suggesting enhanced readout of sensory representation as the mechanism

of VPL. In an interesting study using neurofeedback to investigate causal mechanism of VPL, induced activity in early visual cortex resulted in orientation-specific VPL [20]. The activation patterns in V1/V2 evoked by target orientation stimulus presentation were decoded and repetitively induced in participants with online feedback in the absence of stimulus presentation. Participants' performance on the orientation discrimination task improved after the induction stage. This was interpreted as evidence that V1/V2 plasticity is sufficient for VPL. Motion direction discrimination training was found to increase the decoding accuracy in motion-sensitive area V3A together with connectivity from V3A to intraparietal sulcus (IPS) [21]. This suggests that both sensory representation in early visual areas and readout of this representation by decision-making areas were changed by VPL.

Another area of VPL research investigates structural plasticity that accompanies functional changes associated with performance improvement. This can be achieved on the cellular level thanks to the advancements in optical imaging technology. In a longitudinal study investigating changes to long-range horizontal connections in V1 of monkeys during training with a contour detection task, axonal sprouting and pruning at the trained location were observed [22], similar to a previous report of axonal plasticity in a retinal lesion model by the same group [23]. The authors proposed that VPL arises from the contextual interactions between feedback and horizontal connections. Dendritic spine density in layer 2/3 pyramidal neurons in V1 was found to increase as a result of training with a pattern discrimination task in a mouse model of VPL [24]. The performance improvement partially transferred to the untrained eye and untrained stimulus orientations. It is known that layer 2/3 pyramidal neurons receive feedback from higher cortical areas. This led the researchers to suggest that VPL involves higher cortical areas in addition to V1.

Non-invasive investigation of VPL-dependent structural changes in human participants was carried out using diffusion weighted imaging (DWI). Following up on the seminal study that revealed the increased activation in V1 turns to baseline in later phases of VPL [17], it was found that white matter structure of the inferior longitudinal fasciculus (ILF) was changed after training with texture

discrimination task[25]. ILF is an association tract that connects occipital lobe and anterior temporal lobe. Functional connectivity analysis between V1 and anterior cortical areas revealed increased connectivity suggesting that structural and functional changes were in coordination. The authors proposed a two-phase model of VPL where V1 plasticity that mediates the early phase is followed by structural and functional connectivity changes that support the retention phase.

After decades of research, the mechanism and locus of VPL are still debated. A couple points regarding the seemingly conflicting results emerge from the literature reviewed here. Most notably, many types of different stimuli are used to investigate VPL. Given the functional specialization of visual cortex, it is reasonable to assume that the involved visual areas will differ depending on type of the stimulus. Even when studies report using the same type of stimulus, the experimental procedure as well as task difficulty can greatly vary. Both increased training [26] and increased task difficulty [3] leads to more specific VPL and possibly require the engagement of different neuronal mechanisms. Longitudinal neuroimaging studies provide evidence that different forms of plasticity underlie different phases of VPL [17, 25]. It is possible that some of the conflicting results are due to differences in time points the measurements are made. Taken together, the variety of experimental parameters used in VPL research makes it difficult to piece together the accumulated evidence and get the full picture.

The differences between two methods that predominantly used to investigate neural correlates of VPL constitute another point to consider. Neurophysiological recordings and fMRI measure different aspects of brain activity. Neurophysiological recordings mentioned in this literature review measure spiking activity of individual neurons whereas activity of millions of neurons contributes to fMRI activation in a single voxel. In addition to the scale difference, as it is briefly explained before, it is possible that fMRI is blind to spiking or output activity of neurons and instead measures input activity. The comparison of findings from these two literatures is therefore not straightforward. One possible approach is to integrate the findings from neurophysiological research to computational models used in fMRI analysis. This kind of model-based fMRI approach has the potential to bridge the gap between two literatures.

Another point concerns the use of animal models in neurophysiological research due to the invasive nature of the technique. First of all, it is not yet known whether mechanisms of VPL differ across species. Furthermore, regardless of possible interspecies differences, the use of animal models requires different experimental procedures than studies on humans. Most studies with non-human primates are conducted with awake-behaving animals. However, in some cases, anesthetization of the animal might be necessary for recording, which in effect renders the experimental condition to passive viewing. Active engagement with task and passive exposure to the stimulus are subject to different levels of top-down influences. In fact, it is suggested that passive exposure induces changes at lower-levels whereas task-relevant learning involves changes to multiple levels [27]. Moreover, unlike human studies, VPL in animal models takes extended periods (usually months) of training and occurs through rewards. All in all, differences in experimental procedures warrant another caution to direct comparison of findings from neurophysiology and fMRI literatures.

The aforementioned points raise the possibility that controversy over the mechanism and locus of VPL might be due to a failure to identify different aspects of VPL. A more recent theoretical framework offers reconciliation to the discrepancy in the literature by incorporating feature-based and task-based plasticity together. In the dual plasticity model, both refined sensory representation and improved processing of task-relevant information underlie VPL [28]. To test the validity of this model, participants trained in a motion detection task were scanned both while they were performing the task and while they were passively exposed to the feature [29]. The pattern-classification analysis revealed changes in response to trained stimulus in V1, V3A, and IPS when the task was engaged. However, only V3A showed response changes in the passive exposure condition. The authors concluded that V3A was the locus of feature-based plasticity whereas V1 and IPS had roles in task-based plasticity. Although the dual plasticity model can explain contradictory results in the literature, further investigation is necessary to reveal the effect of different tasks or experimental procedures.

Through decades of research dedicated to determining the brain regions altered by VPL, supporting evidence has been accumulated for a variety of candidates.

Early visual areas, higher visual areas, decision making regions, and connectivity between visual cortex and decision making regions have been considered as the locus of VPL-induced plasticity. The recent effort in VPL research has been directed towards understanding VPL as a product of distribution of plasticity in multiple brain regions along with effect of attention, reward, and feedback in contrast to earlier research which focused on specific brain regions. The existing literature establishes that it is crucial to evaluate the findings together with the details of the experimental procedure to prevent misleading inferences. Understanding the nature of functional and structural plasticity that underlies VPL is important not only because of the theoretical implications but also the potential use of VPL as a treatment for visual impairments. Longitudinal investigations have great importance here in order to reveal the dynamics of VPL-induced plasticity and differentiate between transient and persistent changes.

1.2 Scope of the Present Study

In this study, we investigated VPL-induced plasticity in the visual cortex. For behavioral training, we used bisection discrimination task, a well-established paradigm in the VPL literature. We collected MRI data at three time points during the experimental timeline: before training, approximately midway through training, and after training to assess VPL-dependent changes over the course of learning. Chapter 2 outlines the experimental procedure and presents the results of the behavioral training.

Functional changes were examined with population receptive field (pRF) analysis, a biologically-inspired model-based fMRI analysis method. pRF model is based on decades worth of evidence from neurophysiological research of the receptive field properties of the visual cortex. This analysis approach allows characterization of the response properties of neuronal populations within each voxel and therefore examination of the functional architecture of the visual cortex at a finer scale. We used pRF analysis to reconstruct visual field maps and to estimate pRF sizes in our regions of interest. The method and results of the pRF analysis

are given in Chapter 3.

We collected DWI data to investigate structural changes. Specifically, we assessed microstructural changes in the visual cortex with NODDI (neurite orientation dispersion and density imaging), a DWI-based modeling technique that allows noninvasive imaging of tissue microstructure. To our knowledge, this is the first microstructural level study of VPL-induced plasticity in the human visual cortex. Our analysis pipeline and results are presented in Chapter 4.

Model-based computational neuroimaging approach employed in this study enables a fine-scale investigation of brain function and structure. This approach has the potential to relate better to findings from invasive procedures on animal models and therefore reduce the gap between neuroimaging studies and animal studies. By investigating the whole visual cortex, we aimed to identify which level of the visual processing hierarchy changes through VPL. Furthermore, we examined the dynamics of VPL-induced plasticity through the longitudinal aspect of the study. Overall, this study offers a step towards an in-depth analysis of experience-dependent neuroplasticity in the human visual cortex.

Chapter 2

Experimental Procedure

The data presented in this thesis were collected as a part of a research project our group is working on. The project aims to identify the changes to the brain function and structure over the course of VPL by taking a longitudinal approach and employing a broad range of neuroimaging techniques. Both threshold measurements and MRI sessions were conducted before the training started (pre-training), after three training sessions (mid-training) and once the training has been completed (post-training). The experimental timeline can be seen in Figure 2.1.

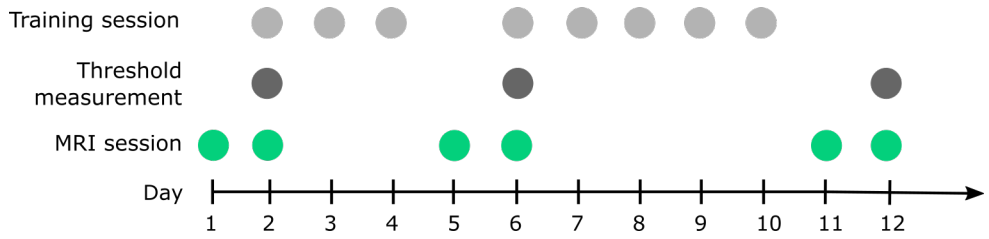

Figure 2.1: Experimental timeline. Behavioral training consisted of eight sessions. Perceptual threshold measurements and MRI sessions were conducted at three different time points during the experiment (pre-, mid-, and post-training). MRI protocols were split over two days due to time constraints (first day: high-resolution T1 image, resting-state fMRI, task-based fMRI, functional localizer; second day: pRF runs, DWI).

MRI sessions were held on two consecutive days because it was not feasible to collect all MRI data in a single session. On the first day, high-resolution T1 image, resting-state and task-based fMRI data were collected. Functional localizer scan was also acquired on the first day. fMRI data for pRF analysis and DWI data, which are the focus of this thesis, were collected on the following day. Each MRI session took about 1-1.5 hour. The participants did not receive any training between these consecutive sessions. Accordingly, they will be referred to as a single session from now on in the text.

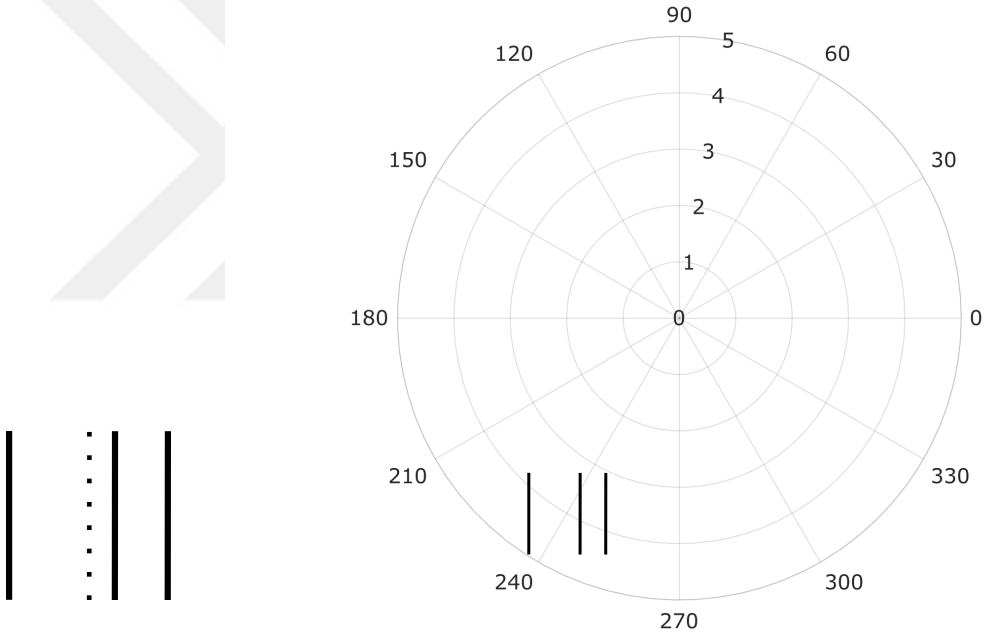

(a) Stimulus (b) Training Location

Figure 2.2: Bisection Discrimination Task. The stimulus consisted of an off-center middle line and two flanking lines (a). The participants determined the displacement of the middle line relative to the center. The training stimulus was presented at 4° eccentricity and 240° polar angle (b). Two control locations were at 300° and 45° polar angle at the same eccentricity as the training location.

The participants were trained with three-line bisection discrimination task where they were asked to determine the displacement of the target line relative to the midline of two flanking lines (Figure 2.2a). The stimulus was presented at 4° eccentricity and 240° polar angle (7 o'clock) (Figure 2.2b). The area spanned by the stimulus was approximately 30° and remained in between 3°-5° eccentricity.

Two control locations were determined as 300° (5 o'clock) and 45° (north-east) polar angle at the same eccentricity as the training location.

The training consisted of eight sessions with 1200 trials per session. A single training session was held in each day since sleep is established as an important factor of performance improvement in VPL [30, 31]. By the same token, the participants were scanned the following day after the relevant part of the training was completed. MRI session was followed by a training session in the second (pre-training MRI session - first training session) and sixth days (mid-training MRI session - fourth training session) for time efficiency.

2.1 Participants

Six participants took part in the experiment (1 author; age range: 18-30, $M = 23.5, SD = 4.46$; 1 male; 1 left-handed). All participants had normal or corrected-to-normal visual acuity. Participants gave their written informed consent to take part in the study. All procedures were approved by Bilkent University Ethics Committee for Research with Human Participants. Participants were financially compensated for their time.

2.2 Behavioral Training Results

We investigated the effect of training by comparing the mean perceptual threshold at the training and control locations in pre-, mid-, and post-training sessions. A two-way repeated measures ANOVA was conducted to determine if there was a change in mean perceptual threshold as a result of the interaction between session and location. The results, given in Table 2.1, revealed that there was no significant interaction between session and location. However, there was a main effect of location which was further examined with post-hoc pairwise comparisons (see Table 2.2). Mean perceptual threshold at the training location

(240° polar angle) and the control location at 300° polar angle was significantly different than control location at 45° polar angle.

Table 2.1: rm-ANOVA Table - Performance Improvement

Cases	Sum of Squares	df	Mean Square	F	p
Session	17.882	2	8.941	2.758	0.111
Residuals	32.413	10	3.241		
Location	96.362	2	48.181	46.499	< .001
Residuals	10.362	10	1.036		
Session * Location	19.859	4	4.965	2.204	0.105
Residuals	45.041	20	2.252		

Note. Type III Sum of Squares

The descriptive plots of perceptual threshold changes at training and control locations, shown in Figure 2.3, revealed an unexpected trend for 240° polar angle (Figure 2.3a) where perceptual thresholds decreased with training up to mid-training threshold measurement but returned to pre-training values in post-training threshold measurement. This trend is evident in both the individual data and mean across the subjects. Typically in a VPL experiment, performance improves drastically as a result of initial training and eventually reaches a saturation level. Therefore, we were expecting much of the performance improvement to occur in the early training sessions and performance to stabilize in the later training sessions. However, in contradiction with the literature, we observed the performance improvement to diminish with ongoing training. There was no chance during our study to detect this unexpected behavioral effect we observed here since the behavioral data and MRI data were collected simultaneously.

Table 2.2: Performance Improvement Post Hoc Comparisons - Location

		Mean Difference	SE	t	p_{holm}
240°	300°	0.007	0.339	0.019	0.985
	45°	-2.830	0.339	-8.342	< .001
300°	45°	-2.837	0.339	-8.361	< .001

Note. P-value adjusted for comparing a family of 3
Note. Results are averaged over the levels of: Session

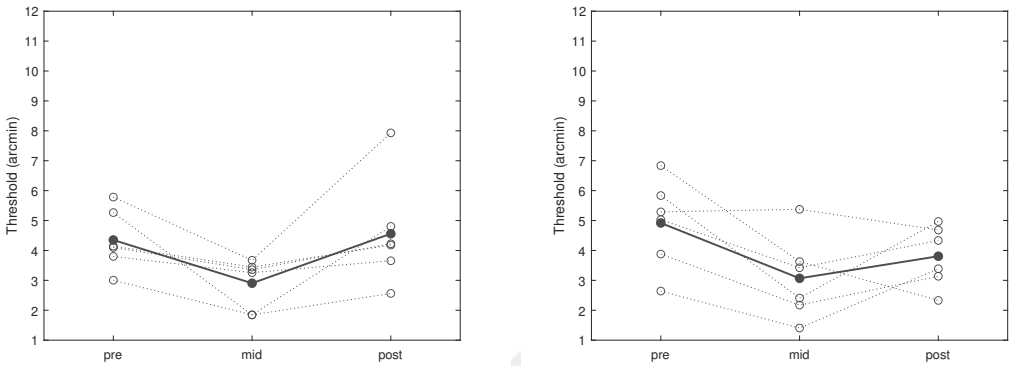

(a) 240° polar angle

(b) 300° polar angle

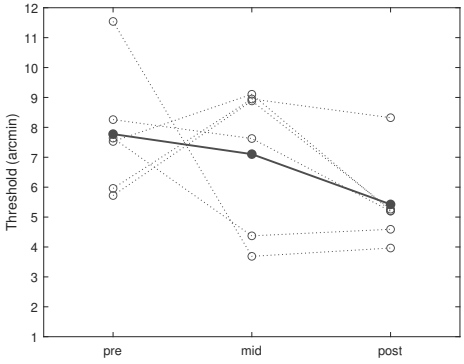

(c) 45° polar angle

Figure 2.3: Perceptual thresholds at the training (a) and control (b and c) locations. The dots show the mean values across all subjects, and the rings are individual mean for each subject.

Interestingly, a similar trend was also observed in the control location at 300° polar angle (Figure 2.3b) which is the mirror-symmetric of the trained location in the contrahemisphere. The other contrahemispheric control location (Figure 2.3c) did not show such trend. Interhemispheric homotopic connections (connections between equivalent regions of each hemisphere) might be responsible for this same pattern emerging in mirror-symmetric locations in the visual cortex.

2.3 MRI Data Acquisition

We used multiband (MB) sequences provided by the Center for Magnetic Resonance Research (CMRR), University of Minnesota, Minneapolis for both functional and diffusion weighted scans. Imaging protocols were adapted from Human Connectome Project and optimized for 3T MRI scanner using available guidelines [32]. This approach allowed us to shorten acquisition time with comparable image quality.

MRI sessions were held at National Magnetic Resonance Research Center (UMRAM), Bilkent University, Ankara. MRI data were collected on a Siemens Tim Trio 3T scanner with a 32-channel phase array head coil. The participants' heads were supported using foam padding to minimize motion during image acquisition. The stimulus was presented on an MRI compatible LCD screen (TELEMED, 1920×1080 pixel, 32 inch) placed at the back of the scanner bore. The participants viewed the stimulus display via a mirror system mounted on top of the head coil. The total viewing distance was measured as 168 cm. The position of the screen was marked and kept constant across participants and sessions. The participants' response was collected with a fiber optic response box (fORP 904 fMRI trigger and response system, 4 Button Bimanual HHSC-2x2, Current Designs). Further details about MRI data acquisition protocols are given in the relevant chapters.

Chapter 3

Population Receptive Field Analysis

3.1 Background

The visual system has a topographic organization. Visual information is conveyed to the visual cortex in an orderly fashion such that adjacent points in the visual field are projected to adjacent positions in the retina, the lateral geniculate nucleus, and the cortex. The topographic representation of the visual field or retinotopy is the fundamental principle for functionally defining boundaries between visual areas. V1 contains a complete and continuous representation of the contralateral visual hemifield and lies along the calcarine sulcus. V2 and V3 have discontinuous hemifield representations which further divides the hemifield to quarter-fields dorsal (V2d, V3d) and ventral (V2v, V3v) to V1. Thus, the boundaries between the visual areas correspond to vertical (V1/V2 boundary) and horizontal (V2/V3 boundary) meridians of the visual field. Angular stimuli such as rotating wedge reveal these boundaries at polar angle reversals. Cortical architecture can also be indicative when delineating visual areas as the vertical meridian is usually represented on gyri, whereas the horizontal meridian is represented in sulci[33].

Another dimension of the retinotopy is eccentricity. Annular stimuli are used to map eccentricity along the visual cortex. Cortical representation of eccentricity moves central to periphery in the posterior-anterior direction with the center of gaze represented at the posterior end of the occipital lobe. The retinotopic representation, however, is distorted as projections from the center of the gaze, foveal projections, occupy disproportionately large cortical surface. Moreover, the cortical surface devoted to a visual degree decreases as a function of eccentricity. This is called cortical magnification.

Imaging V1-V3 maps is fairly straightforward thanks to their highly retinotopic organization. Mapping the extrastriate cortex, on the other hand, proves to be a challenge partly due to the hierarchical nature of visual processing. As we go up in the visual processing stream, inputs from earlier levels converge in higher levels, allowing integration of visual information. Accordingly, the receptive field size increases in higher-level visual areas. This results in smaller retinotopic maps which are more difficult to identify.

The hierarchical organization posits an additional challenge with regard to effective retinotopic stimulus. Early visual areas respond to low-level stimulus features such as contrast, orientation, or contours. At each stage of the visual hierarchy, information from earlier stages is integrated to process more complex features of the visual stimulus. Thus, the traditional retinotopic stimuli, which are typically rendered with high-contrast patterns such as flickering checkerboard pattern and elicit a high response in early visual areas, are not effective at imaging the extrastriate retinotopic maps.

In this study, we used population receptive field (pRF) method to analyze retinotopic maps [34]. pRF refers to the combined receptive field of the population of neurons within a given voxel and is defined with a two-dimensional Gaussian model,

$$g(x,y) = exp\left(-\frac{(x-x_0)^2+(y-y_0)^2}{2\sigma^2}\right) \tag{3.1}$$

where (x_0,y_0) is the pRF center and σ is the pRF size. The neuronal response can

be predicted since the time course of stimulus presentation, $s(x, y, t)$, is known. The predicted blood oxygenation level-dependent (BOLD) response is estimated by convolution of the predicted neuronal response with a hemodynamic response function (HRF). The optimal pRF parameters are then determined by minimizing the errors between the predicted and observed BOLD response. pRF parameters are defined in stimulus space.

pRF method reconstructs the retinotopic maps with greater spatial precision as compared to conventional retinotopy methods. However, the major advantage of pRF modeling over conventional retinotopy methods is the ability to estimate pRF size. There is a fundamental relationship between receptive field size and eccentricity: receptive field size increases with eccentricity within each retinotopic map. This relationship can be observed with pRF analysis as the increase in pRF size as a function of eccentricity [35]. Moreover, pRF size estimates have been shown to be in agreement with neurophysiology measurements in V1-V3 maps[34].

We used pRF analysis both for pRF size estimation and for visual area delineation. By using visual area boundaries, we were able to further specify our regions of interest (ROI) on the basis of visual areas and to focus our investigation of VPL-induced plasticity on these ROIs. Here, we investigated training-induced changes in pRF size in training and control locations. Smaller receptive fields are associated with better visual acuity (e.g. sharp central vision at the fovea). By the same token, decrease in receptive field size might underpin increased ability to discriminate simple visual attributes in VPL. Alternatively, increased receptive field size might improve spatial discrimination through pooling of the activity from neurons with overlapping receptive fields.

3.2 Methods

3.2.1 Participants

Participants were the same as detailed in Chapter 2. One participant of the six that participated in the experiment was excluded due to poor activation in the functional localizer scan. Another participant whose mid-training data was missing was excluded for consistency in repeated measures design. Four participants were included in the remaining steps of the study (1 author; age range: 18-27, $M = 22.75, SD = 3.77$).

3.2.2 Stimulus

We used natural scenes which are rich in visual information and thus potentially more effective than conventional high-contrast stimuli for mapping higher visual areas. We preferred simultaneous wedge and ring stimulus configuration which provides consistent estimates and good model fits with shorter scan durations [36]. The resulting mapping stimulus, a combined wedge and ring stimulus carrying natural images, is previously shown to result in pRF estimations reliable across sessions [37]. This mapping stimulus, especially in terms of intersession reliability, serves well for purposes of our study.

To create the mapping stimulus, the natural images were masked with an aperture consisting of a wedge and a ring. The image presented within the aperture changed every 1 s. The wedge completed a full circle in 60 steps and circled 3 times per run. The ring swept through 36 eccentricity bands in each cycle and completed 5 cycles per run. Each step of the simultaneous wedge and ring stimulus was presented for the duration of 1 TR (2 s). The maximum stimulus radius was 6.75° of visual angle. The wedge rotated a clockwise direction and the ring contracted during odd-numbered runs and vice versa during even-numbered runs. Note that the reporting of clock directions is according to the mirror image the participants viewed during MRI sessions. The stimulus presentation protocol is

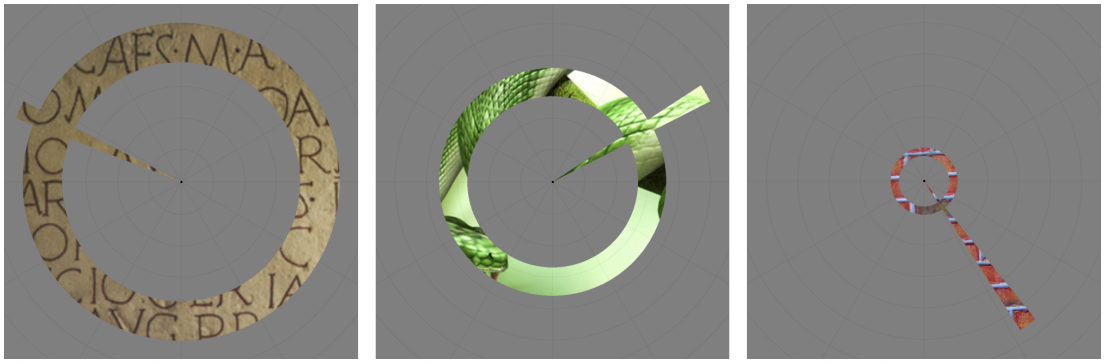

(a) Snapshots of the mapping stimulus

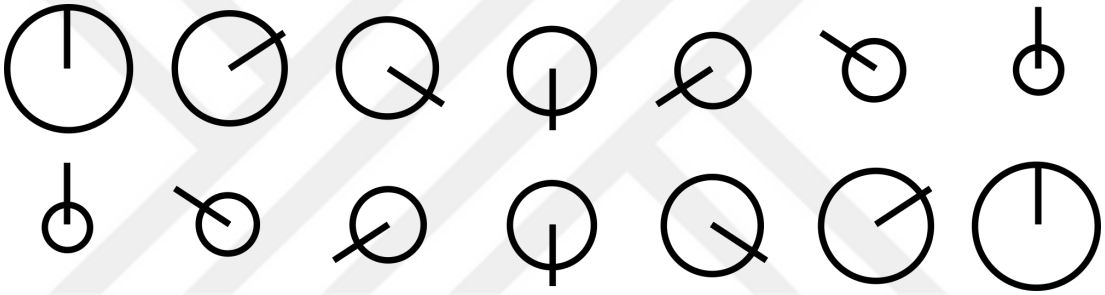

(b) Scheme of alternating stimulus directions

Figure 3.1: Stimulus presentation protocol. The mapping stimulus consisted of natural images masked with a combined wedge and ring aperture (a). In the odd-numbered runs the wedge rotated clockwise and the ring expanded (b, top). In the even-numbered runs the wedge rotated counterclockwise and the ring contracted (b, bottom).

illustrated in Figure 3.1.

Participants were instructed to fixate on a black fixation point presented at the center of the screen at all times. In addition, a low-contrast spider web pattern covering the entire screen was presented together with the fixation point to further facilitate fixation stability. The fixation point changed color with a 0.1 probability in every 200 ms epoch. To ensure fixation compliance, participants were instructed to report color changes (red or green) by pressing corresponding buttons on the response box. Mean percentage correct responses and standard deviations for each participant averaged across runs in each session is given in Table 3.1. We experienced a problem registering responses at one session. Other than that mean correct response percentages were above 75% for every session

indicating good central fixation.

Table 3.1: Fixation Task Results

	Pre-training		Mid-training		Post-training	
Subject	Mean	SD	Mean	SD	Mean	SD
Sub-02	79.83	2.61	86.65	2.44	89.9	3.09
Sub-04	88.39	1.74	89.06	2.86	90.01	1.88
Sub-05	1.76	0.72	82.32	5.9	87.57	1.17
Sub-07	88.13	4.73	89	2.9	89.28	3.57

3.2.3 MRI Acquisition Parameters

T1-weighted structural images were obtained using the 3D MP-RAGE sequence (TR=2600 ms, TE=2.92 ms, flip angle=12°, FoV read=256 mm, FoV phase=87.5% , 176 slices with 1×1×1 mm^3 resolution). pRF runs were collected using the CMRR MB accelerated EPI sequence with following parameters: TR=2000 ms, TE=42.8 ms, MB factor=4, flip angle=80°, FoV read=192 mm, FoV phase=100.0%, partial Fourier factor=7/8, EPI factor=120, 76 slices with 1.6×1.6×1.6 mm^3 resolution. Each pRF run contained 180 measurements and five dummy scans with a total acquisition time of 6 min 22 s. Eight pRF runs were collected in each session.

3.2.4 MRI Data Analysis

3.2.4.1 Preprocessing

Cortical reconstruction and volumetric segmentation of high resolution T1-weighted images was performed with the FreeSurfer v6.0.0 software package (http://surfer.nmr.mgh.harvard.edu/). Dummy volumes of each pRF run were deleted to ensure signal stability. Functional images were realigned and unwarped to correct for head motion and coregistered to the structural scan using SPM12

(http://www.fil.ion.ucl.ac.uk/spm/). The time series at each voxel was linearly detrended and z-score normalized using built-in functions on MATLAB 2017a (Mathworks Inc., Massachusetts, USA). The time series were then averaged across runs separately for both stimulus directions. Next, the averaged time series for two directions were concatenated resulting in a time series with 360 measurements in total. Finally, the data were projected from voxels in the volume space to vertices on the reconstructed surface with a nearest-neighbor interpolation using the FreeSurfer software package. The preprocessing pipeline is illustrated in Figure 3.2.

3.2.4.2 pRF Analysis

pRF model fitting was performed using SamSrf 6.05 (http://osf.io/2rgsm/) on MATLAB 2017a (Mathworks Inc., Massachusetts, USA). The binary image of the stimulus aperture indicated the position of stimulus at each time point. The canonical HRF based on previous empirical data fit to a double gamma function [38] as implemented in SamSrf was used to predict the BOLD signal. The pRF parameters were estimated with a coarse-to-fine optimization approach on unsmoothed data. Surface calculations were then carried out on smoothed data to obtain maps for delineation and visualization purposes. Only vertices with a goodness-of-fit $R^2 > 0.05$ were included in surface calculations. A set of example pRF maps of a representative participant can be seen in Figure 3.3.

Pre-training pRF maps were used to define visual area boundaries except for one participant whose pre-training maps were not eligible for delineation. Mid-training pRF runs were projected onto pre-training reconstructed surface to generate pRF maps of this participant. Visual areas were manually delineated based on polar and eccentricity maps using the delineation tool in SamSrf. We restricted our analysis to early visual areas V1, V2, and V3 in order to ensure consistency since it was not possible to reliably identify further extrastriate areas in all participants.

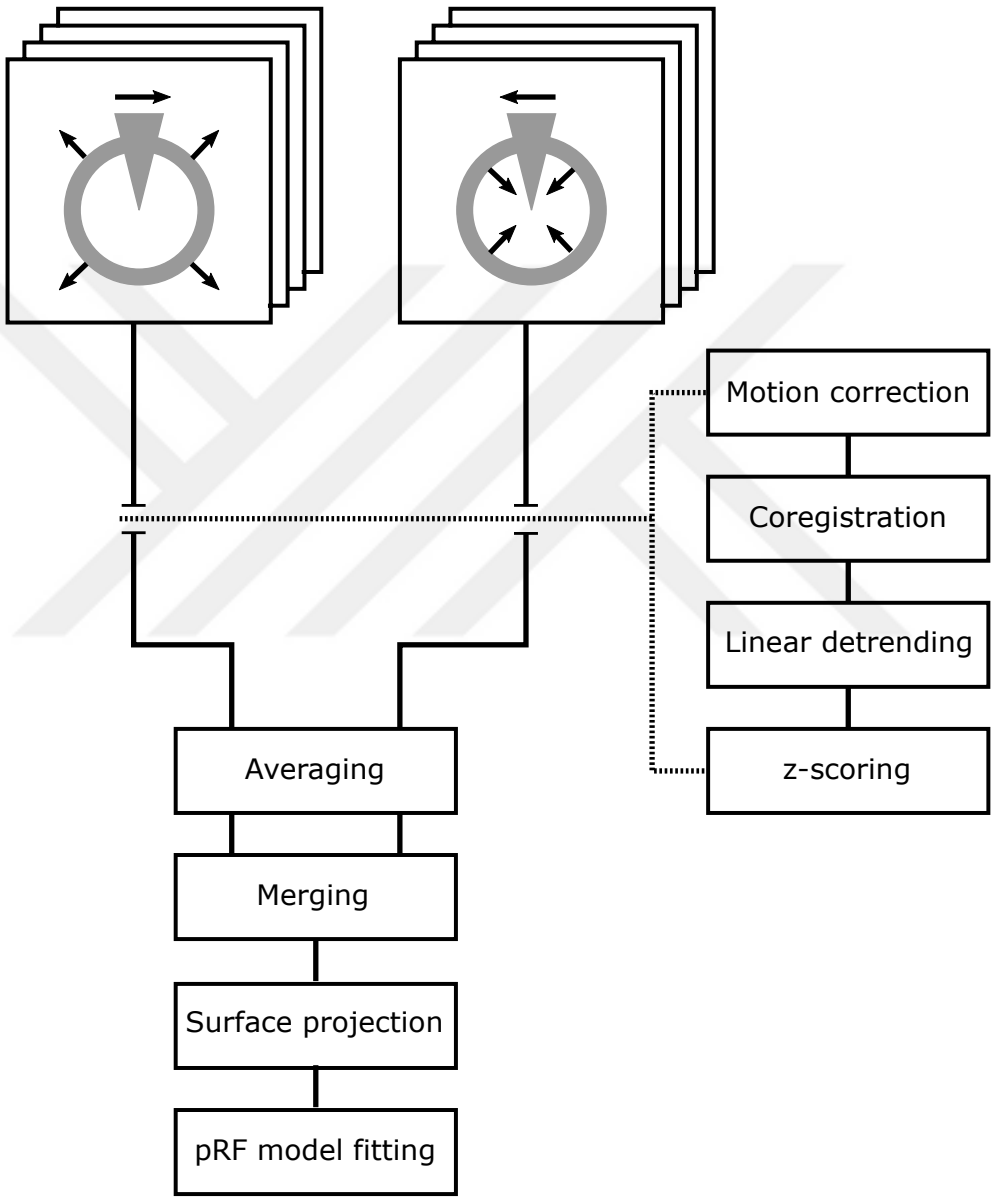

Figure 3.2: pRF Preprocessing Pipeline. After motion correction and coregistration, the time series for each run were z-score normalized and linearly detrended. Next, the time series were averaged separately for two stimulus directions. The resulting averages were then merged together and projected to the reconstructed surface.

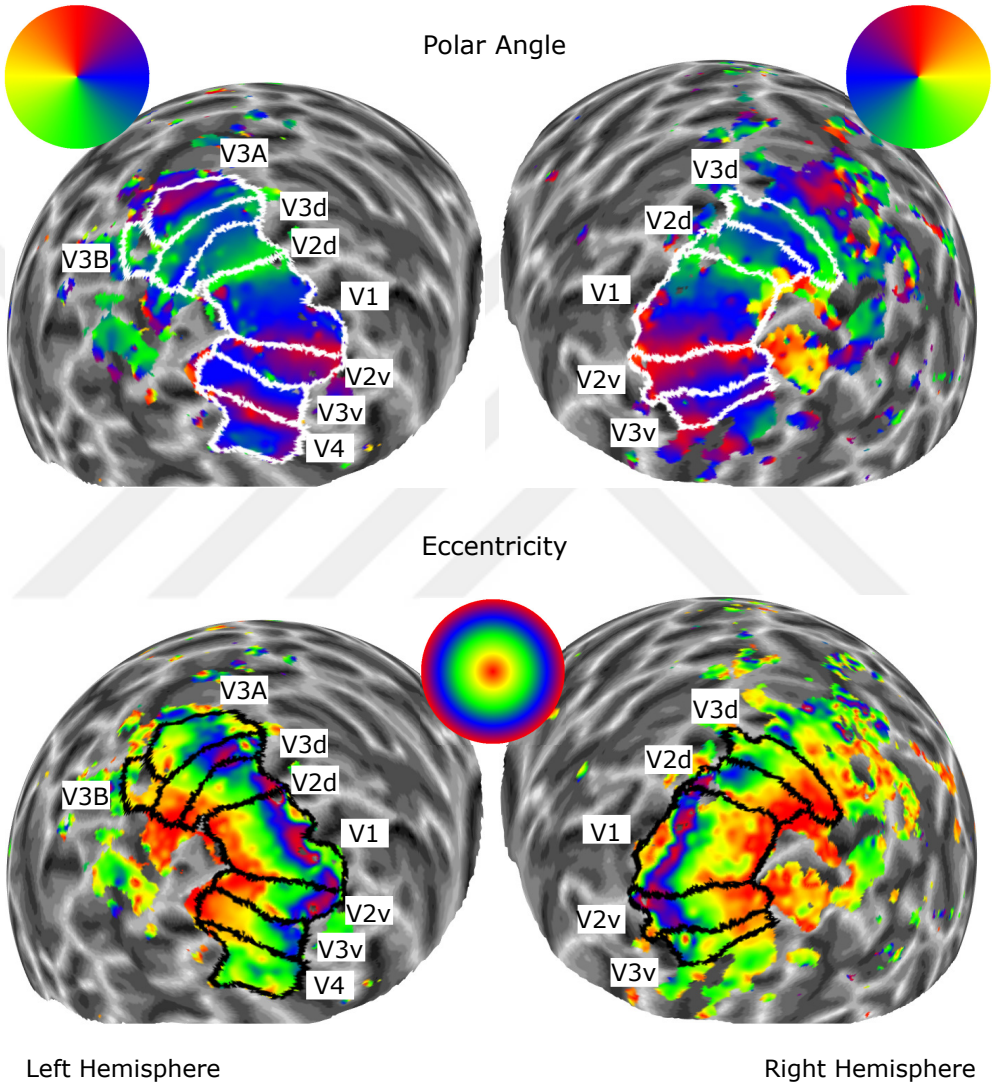

Figure 3.3: Example pRF maps of a representative participant. The maps are generated on a spherical representation of the cortex in order to reveal areas buried in sulci. The polar angle maps are used in visual area delineation (top). The boundaries between the visual areas lie along polar angle reversals. Eccentricity maps show the distance from center (bottom). The maximum eccentricity of the stimulus was 6.75° of visual angle.

3.2.4.3 ROI Identification

We used a functional localizer scan to locate subject-specific ROIs at the training location (240° polar angle) and two control locations (45° and 300° polar angles). A flickering checkerboard with same size as the behavioral task stimulus was presented at one of three locations at each run. The resulting activation cluster was projected onto the reconstructed surface using Freesurfer's tksurfer tool together with visual area labels generated with pRF analysis. The activation was divided manually into visual areas using boundaries of visual area labels. Three functional ROIs (V1, V2, and V3) at each location were obtained as a result. ROI identification pipeline is illustrated in Figure 3.4.

3.2.4.4 Further Analysis

Intersession alignment of functional ROIs were performed with Freesurfer's mri_label2label in the surface space. Estimates of pRF size (σ) and pRF center (x_0,y_0) were extracted at each functional ROI from vertices with a goodness-of-fit $R^2 > 0.15$. Since it was not possible to obtain well-defined ROIs through our functional localization protocol, we further specified the vertices based on the location of pRF centers. Only the pRF centers located between within 15° polar angle proximity of the stimulus presentation location and between 3° - 5° eccentricity bands were included. In this way, we restricted our analysis to pRF estimates located in the area spanned by the behavioral stimulus. An example of pRF estimates satisfying these criteria is visualized in Figure 3.5.

In order to investigate VPL-dependent changes to pRF size, we computed mean pRF size from selected vertices in each functional ROI and compared with each other on the basis of session, location, and visual area. Statistical analysis was performed with JASP (Version 0.12.2)

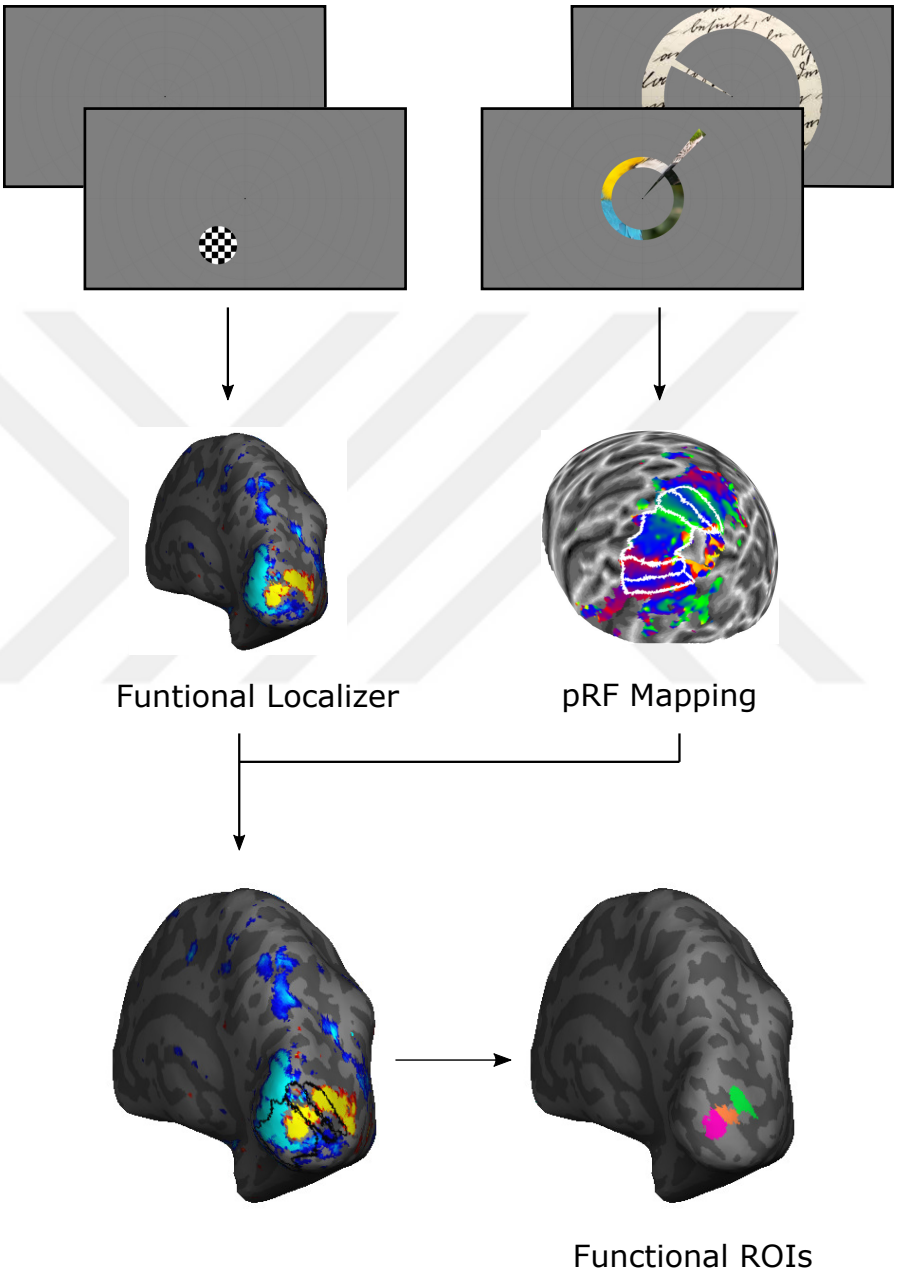

Figure 3.4: ROI Identification Pipeline. The activation yielded by functional localizer was overlaid together with visual area labels obtained from pRF mapping. The functional ROIs were identified at the intersections of activation cluster and visual area boundaries.The pipeline depicts the identification of ROIs at the training location (240° polar angle) (Pink: V1, Orange:V2d, Green: V3d).

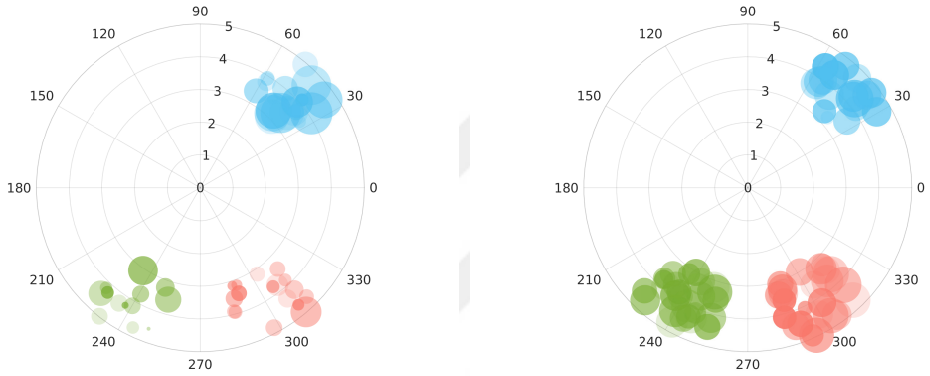

(a) V1

(b) V2

(c) V3

Figure 3.5: Polar plots of pRF estimates of a representative participant at each functional ROI represented in the visual space. Green points represent the pRF estimates with centers located in the training location (240° polar angle). Red and blue points represent pRF estimates at the control locations (red: 300° polar angle, blue: 45° polar angle). The center of each point represents the pRF center. The size of data points is proportional to the estimated pRF size.

3.3 Results

A 3×3×3 repeated measures ANOVA was conducted to investigate the effect of session (pre-, mid-, and post-training), location (240°, 300°, and 45° polar angle), and visual area (V1, V2, and V3) on mean pRF size. The results, given in Table 3.2, do not show any training related differences in mean pRF size. The descriptive plots are given in Figure 3.6.

Table 3.2: rm-ANOVA Table - Mean pRF Size

Cases	Sum of Squares	df	Mean Square	F	p
Session	0.031	2	0.015	1.959	0.221
Residuals	0.047	6	0.008		
Location	0.275	2	0.137	1.349	0.328
Residuals	0.610	6	0.102		
Visual Area	7.155	2	3.578	39.766	< .001
Residuals	0.540	6	0.090		
Session * Location	0.026	4	0.007	0.604	0.667
Residuals	0.132	12	0.011		
Session * Visual Area	0.039	4	0.010	0.585	0.679
Residuals	0.198	12	0.017		
Location * Visual Area	0.318	4	0.080	1.066	0.415
Residuals	0.896	12	0.075		
Session * Location * Visual Area	0.060	8	0.007	1.307	0.287
Residuals	0.137	24	0.006		

Note. Type III Sum of Squares

There was a main effect of visual area on mean pRF size ($F(2, 6) = 39.766, p < 0.001$) as expected. Post-hoc pairwise comparisons for visual area (Table 3.3) indicated that mean pRF sizes in each visual area was significantly different from each other. This result is in accordance with our knowledge of visual hierarchy and expected regardless of VPL.

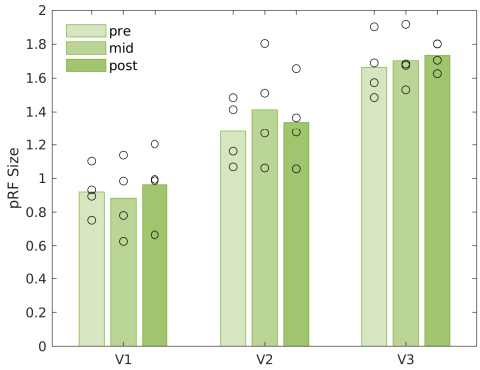

(a) 240° polar angle

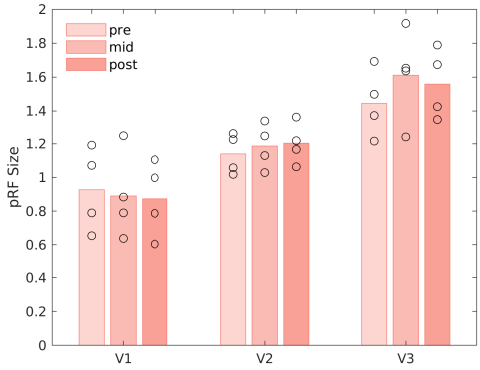

(b) 300° polar angle

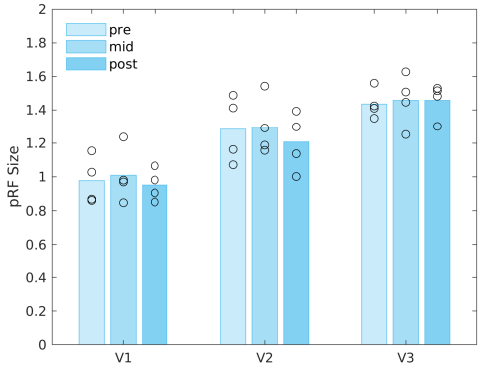

(c) 45° polar angle

Figure 3.6: Mean pRF sizes for each functional ROI at the training (a) and control (b and c) locations. The bars show the mean values across all subjects, and the points are individual mean for each subject.

Table 3.3: Mean pRF Size Post Hoc Comparisons - Visual Area

		Mean Difference	SE	t	p_{holm}
V1	V2	-0.329	0.071	-4.647	0.007
	V3	-0.630	0.071	-8.915	$< .001$
V2	V3	-0.302	0.071	-4.269	0.007

Note. P-value adjusted for comparing a family of 3
Note. Results are averaged over the levels of: Session, Location

3.4 Intermediate Discussion

In this part of the study, we investigated VPL-dependent changes to pRF size in early visual areas V1, V2, and V3. There were no training-related changes in mean pRF size. This finding is consistent with a previous study investigating VPL of bisection discrimination task in monkeys where receptive field size of V1 neurons in trained and untrained animals did not differ [12]. However, given our small sample size, this result is not conclusive and needs to be confirmed with a larger sample.

Unfortunately, we were not able to acquire high-quality retinotopic maps in all participants which prevented us to identify visual areas beyond V1-V3. This calls for further optimization of the imaging protocol to increase the signal-to-noise ratio (SNR). The most straightforward approach to increase SNR would be increasing the run number. However, this is not convenient for our research which already requires long MRI sessions. A more favorable solution for the current research is the optimization of scan parameters without increasing the total acquisition time for example through increasing voxel size and decreasing TR.

Another possible source of failure to identify areas beyond early visual cortex might be that the fixation task was overdemanding in terms of spatial attention. Enhanced response reliability and increased SNR were found with phase-encoded retinotopic mapping when attention is directed to retinotopic mapping stimulus instead of central fixation point [39]. Conversely, it might be possible that high

attentional demand at the central fixation point results in decreased SNR in retinotopic maps. The probability of color change in our fixation task was two to three times higher as compared to studies using similar stimulus configurations [36] [37]. This was done as a precautionary measure to ensure constant fixation in the absence of an eye-tracking system but might cause a counterintuitive effect. A target detection task within the stimulus aperture in combination with a less demanding central fixation task might allocate spatial attention to the retinotopic mapping stimulus and thus provide more reliable visual responses in higher-visual areas.

It is important to note that although SNR was insufficient for identification of higher-visual areas this does not translate to decreased reliability of the pRF estimates in the early visual areas we were able to identify. Nevertheless, confirmation of our findings with a larger sample and further investigation of VPL-dependent changes in higher-visual areas are necessary.

Chapter 4

Diffusion Weighted Imaging

4.1 Background

The fundamental principle of diffusion weighted imaging (DWI) is based on the random Brownian motion of water molecules. When water molecules do not encounter any restrictions they move freely in every direction. This type of motion is called isotropic diffusion. However, in structured spaces such as biological tissue or a piece of paper, the movement of water molecules is directionally restricted or anisotropic. Diffusion anisotropy carries information about the underlying tissue structure. Diffusion of water in highly organized structures such as the white matter is more anisotropic compared to diffusion in less coherent structures such as gray matter. The degree of anisotropy can be quantified using models. Diffusion tensor imaging (DTI), the most widely used DWI method, uses a six-parameter ellipsoid to characterize diffusion [40]. The shape of diffusion ellipsoid provides information about anisotropy. The longest axis of the ellipsoid indicates the principal diffusion direction which is assumed to represent the fiber orientation. The information from the tensor model can be used to generate contrast and reconstruct white matter tracts.

An important limitation of DTI is the assumption of a single fiber orientation

in each voxel. More often than not there are multiple fiber orientations in a voxel due to crossing, fanning or bending fibers [41]. DTI approach can not account for these orientation configurations except for a lower diffusion anisotropy. Higher-order models have been proposed to address this limitation. One such model is constrained spherical deconvolution (CSD) which estimates a fiber orientation distribution at each voxel [42]. CSD-based tractography has been shown to provide biologically reliable mapping in contrast to DTI-based tractography methods which fails to accurately estimate fiber orientations [43]. In our study, we used a CSD-based tractography algorithm to generate white matter tracks between functional ROIs identified as described in the previous chapter.

In addition to macrostructural organization, cellular level structures also contribute to diffusion anisotropy with membranes being the primary determinant [44]. The signal's sensitivity to cellular architecture makes it a promising probe for microstructural imaging. However, the signal in a voxel represents the combination of water diffusion in multiple water compartments where water molecules have different diffusion patterns. These diffusion patterns must be distinguished in order to extract information about the tissue microstructure. Neurite orientation dispersion and density imaging (NODDI) achieves this by combining multi-shell DWI with a two-level multicompartment model [45].

NODDI tissue model differentiates between non-tissue (CSF) and tissue (white matter and gray matter) at the first level by fitting a isotropic diffusion model as the water diffuses freely outside the tissue. At the second level, intra-neurite compartment (the space bounded by membranes of axons and dendrites) is modeled with sticks to reflect the highly restricted diffusion in this space. The orientation distribution of the neurites is represented with the Watson distribution and ranges from highly parallel (e.g. corpus callosum) to highly dispersed (e.g. cortex). The hindered diffusion in the extra-neurite compartment (cell bodies and glial cells) is modeled with an ellipsoid. NODDI returns three summary statistics: neurite density or intra-cellular volume fraction (ICVF) representing amount of neurites, orientation dispersion index (ODI) representing variability of neurite orientations, and isotropic volume fraction (ISO) representing amount of free water. NODDI tissue model is illustrated in Figure 4.1.

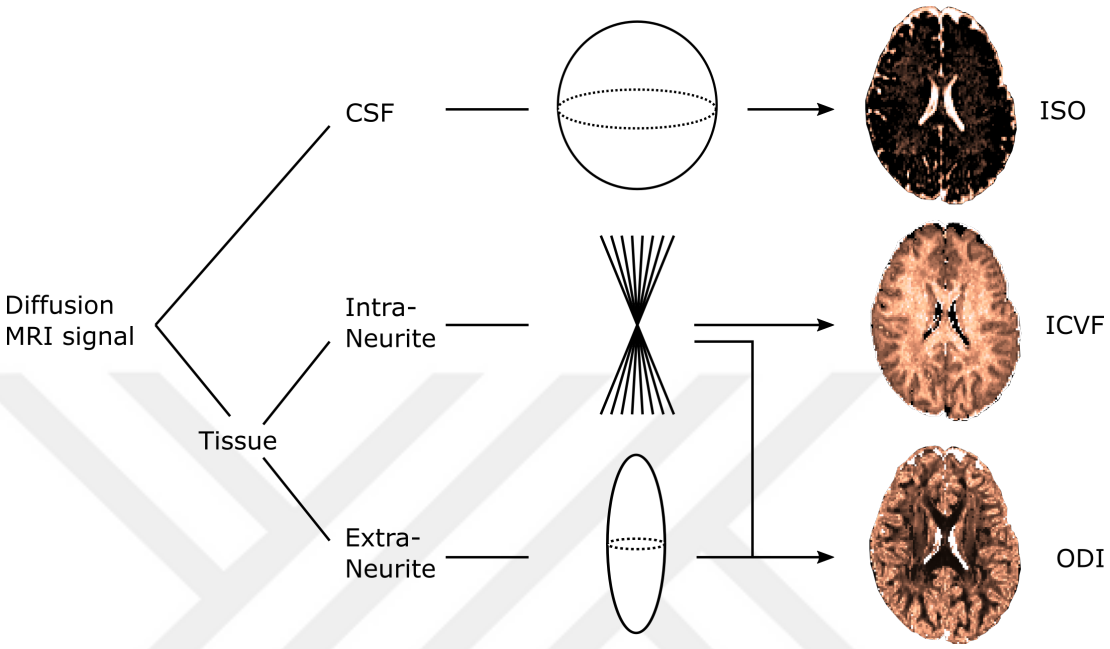

Figure 4.1: NODDI Tissue Model. Diffusion MRI signal is broken down at two levels. At the first level, isotropic diffusion which accounts for CSF is modeled. At the second level, restricted diffusion in the intra-neurite compartment is modeled with sticks and hindered diffusion in the extra-neurite compartment is modeled with an ellipsoid. Three indices are calculated as a result: intra-cellular volume fraction (ICVF), orientation dispersion index (ODI), and isotropic volume fraction (ISO).

The advantage of NODDI over other model-based microimaging techniques is its feasibility. NODDI allows quantification of tissue microstructure with reasonable acquisition time and moderate hardware requirements. Furthermore, NODDI provides robust estimates with comparable scan-rescan reproducibility to DTI [46, 47]. Overall, NODDI emerges as a promising technique to explore longitudinal changes in the brain microstructure.

Here, we used NODDI to investigate training-induced changes both in cortical microstructure and in white matter microstructure. Cortical plasticity refers to the experience-dependent changes in gray matter structure. Based on an expansion-renormalization model of neuroplasticity [48], we predict an initial growth of new connections followed by a selective elimination process by which neuronal circuitry is refined. Such a process might reflect itself in ICVF and ODI with an increase in the early stages of training and a subsequent retreat to

pre-learning values in the later stages.

Complementary to cortical plasticity, white matter can also demonstrate neuroplasticity in response to training. Being a more recently identified phenomenon, the mechanisms of white matter plasticity are not fully disclosed. Possible experience-dependent structural changes in white matter involve new myelin formation, remodeling of existing myelin, and alterations to myelin sheath length. Since myelination is inversely related to the fraction of extracellular space in a given volume, ICVF can indirectly detect differences in myelination. In addition to regulation of myelin, regulation of axonal branching is also suggested as a possible plasticity mechanism although yet to be shown in brain white matter [49]. Both ODI and ICVF indicate changes in axonal branching in the white matter.

4.2 Methods

4.2.1 Participants

Same participants were included here as the pRF analysis ($N = 4$, 1 author; age range: 18-27, $M = 22.75, SD = 3.77$).

4.2.2 MRI Acquisition Parameters

Two sets of diffusion weighted images were obtained using the CMRR MB accelerated EPI sequence in an anterior to posterior phase encoding direction with following parameters: TR=3510 ms, TE=114.4 ms, MB factor=4, flip angle=78°, FoV read=211 mm, FoV phase=86.4%, partial Fourier factor=6/8, EPI factor=114, 76 slices with 1.6×1.6×1.6 mm^3 resolution. The diffusion gradients were generated using MASSIVE gradient tool [50].

Single-shell diffusion weighted data was acquired with 60 diffusion gradient directions using a b-value of b=1000 s/mm^2. Seven images with no diffusion

weighting (b=0 s/mm^2) were interspersed throughout the scan to minimize the signal drift. Total acquisition time was 4 minutes 9 seconds.

Multi-shell diffusion weighted data was acquired with three b-value shells (20 directions in b=1000 s/mm^2, 40 directions in b=1800 s/mm^2, and 60 directions in b=2400 s/mm^2) and eight interspersed b0 images (TA=7 min 47 s). A single b0 image was collected in opposite phase-encoding direction to be used in susceptibility-induced geometric distortion correction of the diffusion weighted images.

4.2.3 MRI Data Analysis

4.2.3.1 Preprocessing

Same preprocessing steps were deployed for both sets of diffusion weighted images. Images were corrected for signal drift using ExploreDTI v4.8.6 [51]. The resulting left-right orientation flip was corrected using FSLUTILS as implemented in FSL v6.0.2 (https://fsl.fmrib.ox.ac.uk/fsl/fslwiki/). Susceptibility-induced geometric distortions were estimated using FSL's topup tool. FSL's eddy tool was used to correct for susceptibility-induced geometric distortions, eddy current-induced distortions and subject movements. The preprocessing pipeline is illustrated in Figure 4.2.

4.2.3.2 ROI Alignment

Functional ROIs identified in the surface space (described under Section 3.2.4.3 on page 26) were converted to volume space via Freesurfer's mri_label2vol. We generated two ROI sets different in the cortical depth they span: deep cortical ROIs and superficial cortical ROIs. An example of deep cortical ROIs and superficial cortical ROIs can be seen in Figure 4.3.

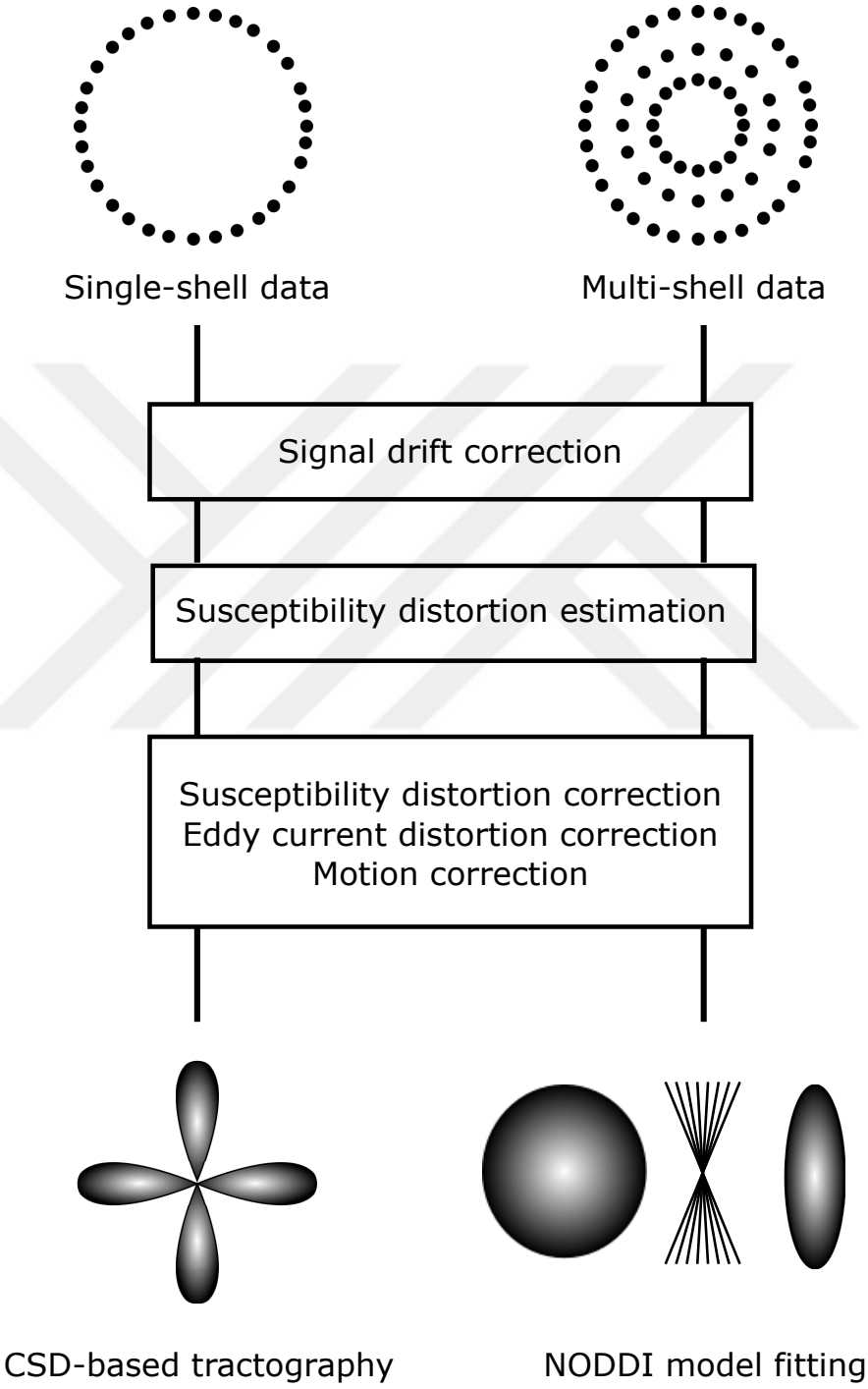

Figure 4.2: DWI Preprocessing Pipeline. Signal drift correction was applied to both single-shell and multi-shell diffusion weighted images as the first step. Next, susceptibility-induced geometric distortions were estimated. The images were then corrected for susceptibility-induced geometric distortions, eddy current-induced distortions and motion. CSD-based tractography was performed on the single-shell data whereas multi-shell data was fit to the NODDI model.

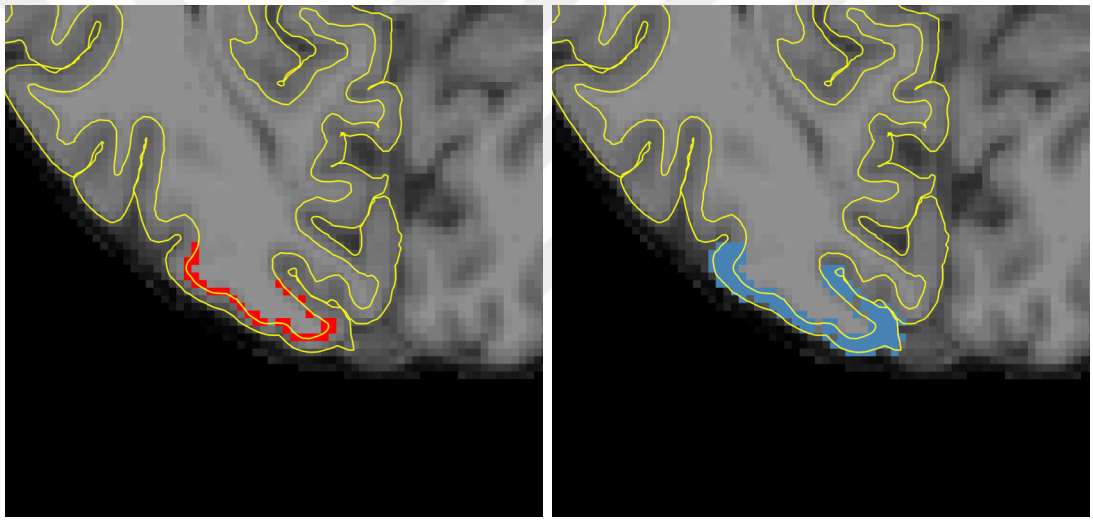

(a) Deep Cortical ROI (b) Superficial Cortical ROI

Figure 4.3: An example of deep cortical ROIs and superficial cortical ROIs. The figure shows functional ROIs (V1, V2, and V3) at the trained location (240°) converted to volume space. Deep cortical ROIs (a) were restricted to proximity of the gray-white matter boundary. Superficial cortical ROIs (b) reached upto the pial surface. Both sets of ROIs are shown here on the high-resolution T1-weighted image for visualization purposes.

Deep cortical ROIs were restricted to deep gray matter close to the gray-white matter boundary (Figure 4.3a). These ROIs were than prepared to be used in tractography analysis by binarizing, indexing and merging together with FSLUTILS. This step resulted in a mask where every ROI has a specific intensity value. Any voxels appearing in more than one ROI were excluded from the mask. This mask served as an atlas in tractography analysis we conducted to reconstruct white matter tracts between functional ROIs.

Superficial cortical ROIs were allowed to reach upto the pial surface (Figure 4.3b). These ROIs used in the investigation of cortical changes in response to training. Intersession alignment of superficial cortical ROIs was achieved with FSL's FLIRT.

4.2.3.3 Tractography Analysis

Whole-brain tractography was performed on the single-shell diffusion weighted data from pre-learning session using the CSD-based tractography algorithm implemented in ExploreDTI with following tracking parameters: $2\times2\times2$ mm^3 seed point resolution, 1 mm step size, 30° angle threshold, 50 - 500 mm fiber length range. Fiber tracts between ROIs were identified and extracted from the whole-brain tractography. We were able to reliably identify the fiber tracts between trained location (240°) and the homotopic control location (300°) in V1 of three participants (1 author; age range: 18-27, $M = 23, SD = 4.58$). These tracts were converted to binarized masks to be used in further analysis. Tractography analysis pipeline is illustrated in Figure 4.4.

4.2.3.4 NODDI Model Fitting

Multi-shell diffusion weighted data was fitted to the NODDI model [45] using AMICO toolbox [52]. Whole-brain ICVF, ODI and ISO maps were generated for all three sessions. Whole-brain NODDI parameter maps of a representative participant can be seen in Figure **??**.

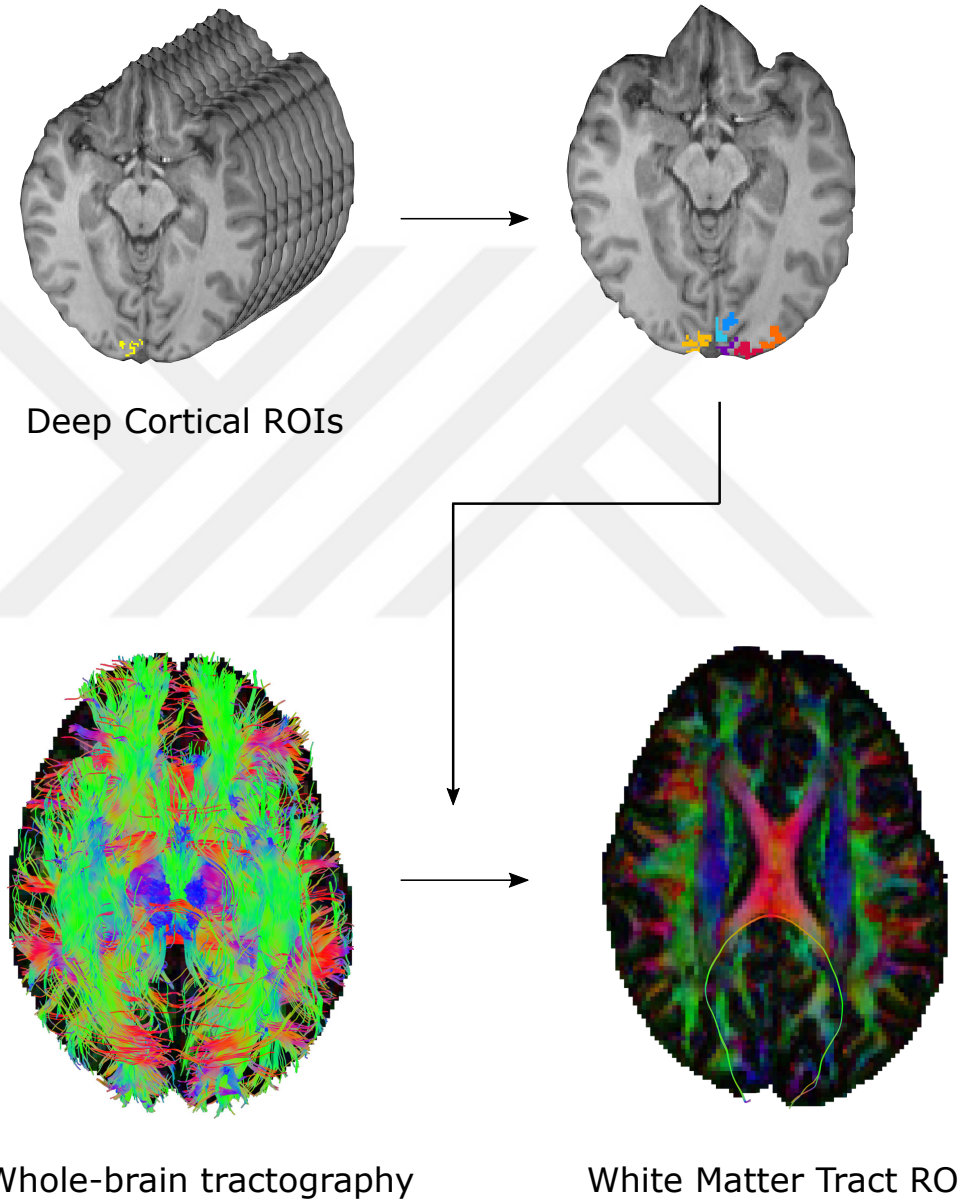

Figure 4.4: Tractography Analysis Pipeline. Deep cortical ROIs were binarized, indexed and merged together in order to serve as an atlas for tractography analysis. Fiber tracts between ROIs were extracted from whole-brain tractography. This analysis resulted in a single white matter tract identified between trained location (240°) and the homotopic control location (300°) in V1.

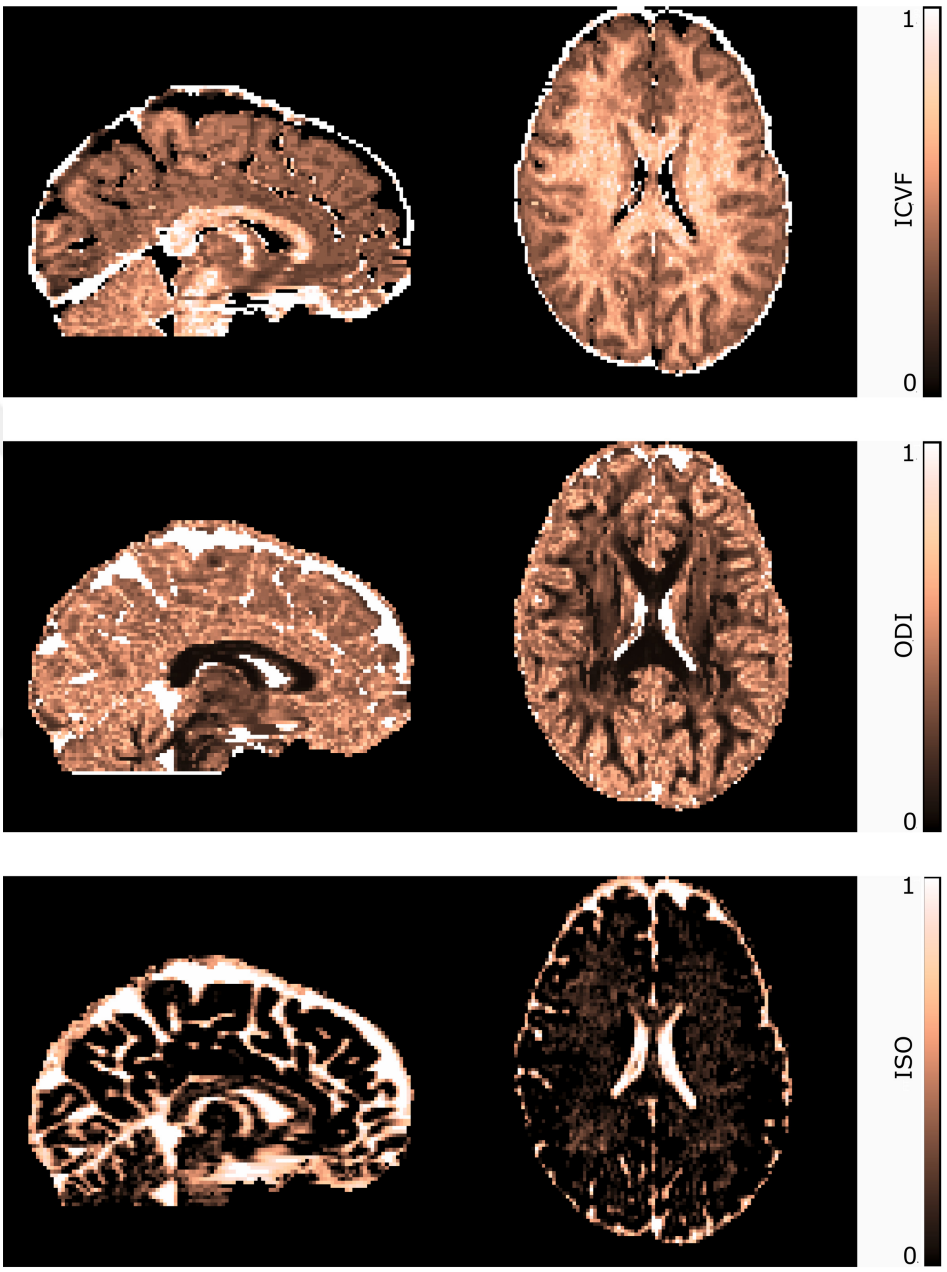

Figure 4.5: Whole-brain NODDI parameter maps of a representative participant. The maps are consistent with our anatomical knowledge of the brain. ICVF map (top) shows a pattern where neurite density is higher in white matter as compared to gray matter whereas ODI map (middle) demonstrates higher orientation dispersion in gray matter than in white matter. ISO map (bottom) shows the highest values at the ventricles.

Table 4.1: rm-ANOVA Table - Mean ICVF

Cases	Sum of Squares	df	Mean Square	F	p
Session	0.004	2	0.002	1.688	0.262
Residuals	0.008	6	0.001		
Location	0.008	2	0.004	0.791	0.496
Residuals	0.032	6	0.005		
Visual Area	0.010	2	0.005	4.831	0.056
Residuals	0.006	6	0.001		
Session * Location	0.008	4	0.002	1.553	0.249
Residuals	0.015	12	0.001		
Session * Visual Area	0.003	4	8.488e-4	0.946	0.471
Residuals	0.011	12	8.975e-4		
Location * Visual Area	0.012	4	0.003	2.416	0.106
Residuals	0.015	12	0.001		
Session * Location * Visual Area	0.006	8	7.879e-4	1.403	0.245
Residuals	0.013	24	5.616e-4		

Note. Type III Sum of Squares

4.2.3.5 Further Analysis

The NODDI indices at the superficial cortical ROIs and at the white matter tract ROI were extracted from whole-brain NODDI parameter maps and averaged within ROIs using FSLUTILS. Training-related changes to NODDI indices were investigated by repeated measures ANOVA tests. Statistical analysis was performed with JASP (Version 0.12.2).

4.3 Results

3×3×3 repeated measures ANOVA tests (session: pre-, mid-, and post-training; location: 240°, 300°, and 45° polar angle; visual area: V1, V2, and V3) did not reveal any training related effects on mean ICVF (Table 4.1), mean ODI (Table 4.2) and mean ISO (Table 4.3) values at the superficial cortical ROIs. Descriptive plots of mean ICVF, ODI and ISO values at each ROI can be seen in Figure 4.6, Figure 4.7, and Figure 4.8, respectively.

Table 4.2: rm-ANOVA Table - Mean ODI

Cases	Sum of Squares	df	Mean Square	F	p
Session	0.001	2	5.622e-4	1.403	0.316
Residuals	0.002	6	4.008e-4		
Location	0.007	2	0.004	2.252	0.186
Residuals	0.009	6	0.002		
Visual Area	0.002	2	0.001	0.900	0.455
Residuals	0.008	6	0.001		
Session * Location	9.770e-4	4	2.442e-4	1.476	0.270
Residuals	0.002	12	1.655e-4		
Session * Visual Area	0.001	4	3.622e-4	0.719	0.595
Residuals	0.006	12	5.038e-4		
Location * Visual Area	0.010	4	0.002	2.088	0.145
Residuals	0.014	12	0.001		
Session * Location * Visual Area	0.002	8	2.385e-4	1.152	0.367
Residuals	0.005	24	2.071e-4		

Note. Type III Sum of Squares

Table 4.3: rm-ANOVA Table - Mean ISO

Cases	Sum of Squares	df	Mean Square	F	p
Session	0.004	2	0.002	0.250	0.787
Residuals	0.052	6	0.009		
Location	0.003	2	0.002	0.102	0.904
Residuals	0.103	6	0.017		
Visual Area	0.147	2	0.073	7.892	0.021
Residuals	0.056	6	0.009		
Session * Location	0.004	4	0.001	0.318	0.860
Residuals	0.042	12	0.003		
Session * Visual Area	9.285e-4	4	2.321e-4	0.186	0.941
Residuals	0.015	12	0.001		
Location * Visual Area	0.021	4	0.005	0.583	0.681
Residuals	0.106	12	0.009		
Session * Location * Visual Area	0.021	8	0.003	1.502	0.209
Residuals	0.042	24	0.002		

Note. Type III Sum of Squares

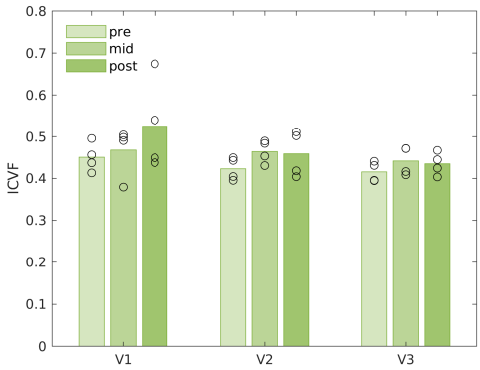

(a) 240° polar angle

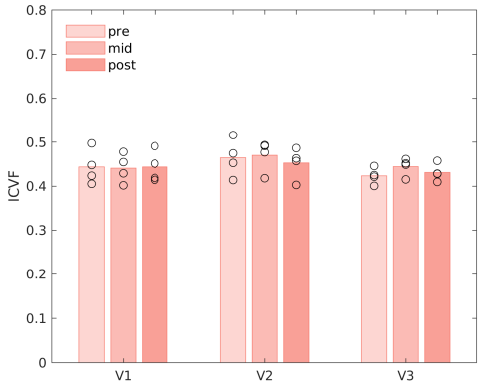

(b) 300° polar angle

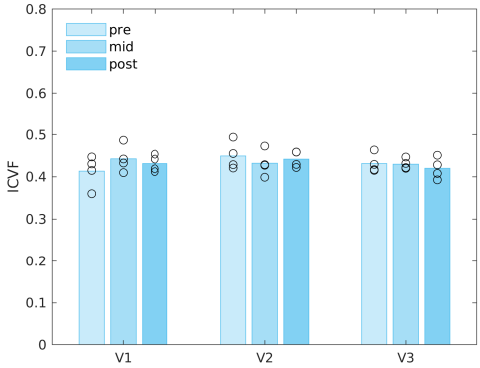

(c) 45° polar angle

Figure 4.6: Mean ICVF at each functional ROI at the training (a) and control (b and c) locations. The bars show the mean values across all subjects, and the points are individual mean for each subject.

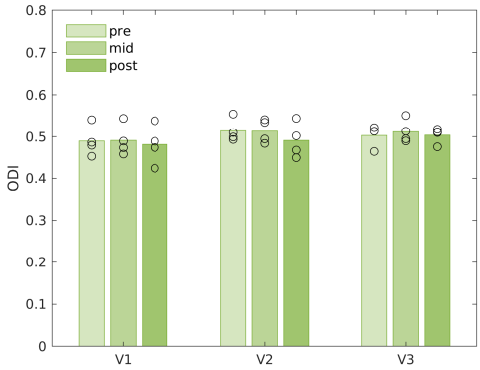

(a) 240° polar angle

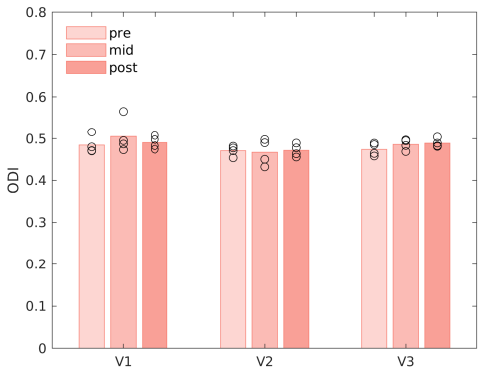

(b) 300° polar angle

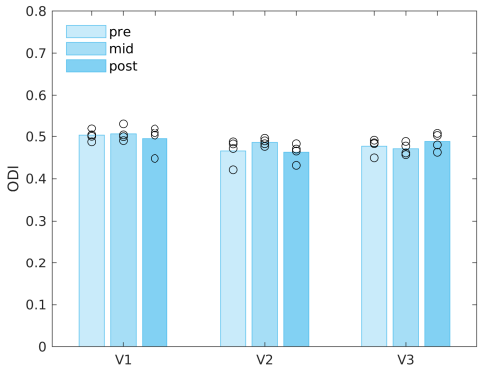

(c) 45° polar angle

Figure 4.7: Mean ODI at each functional ROI at the training (a) and control (b and c) locations. The bars show the mean values across all subjects, and the points are individual mean for each subject.

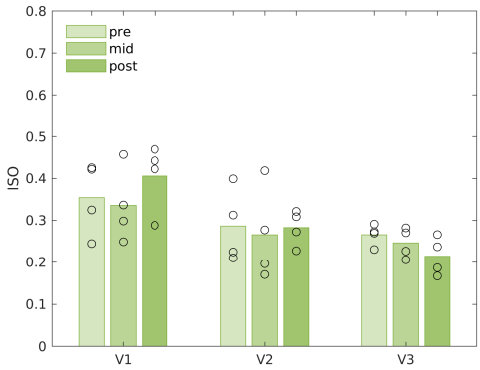

(a) 240° polar angle

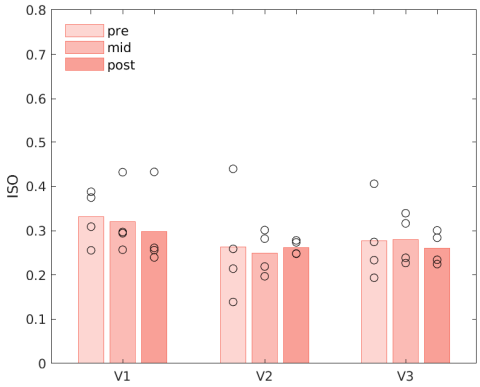

(b) 300° polar angle

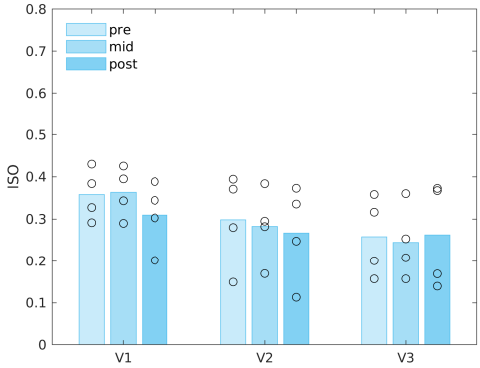

(c) 45° polar angle

Figure 4.8: Mean ISO at each functional ROI at the training (a) and control (b and c) locations. The bars show the mean values across all subjects, and the points are individual mean for each subject.

Table 4.4: Mean ISO Post Hoc Comparisons - Visual Area

		Mean Difference	SE	t	p_{holm}
V1	V2	0.069	0.023	3.018	0.047
	V3	0.085	0.023	3.746	0.029
V2	V3	0.017	0.023	0.728	0.494

Note. P-value adjusted for comparing a family of 3
Note. Results are averaged over the levels of: Session, Location

There was a main effect of visual area on mean ISO ($F(2, 6) = 7.892, p = 0.021$). Post-hoc pairwise comparisons for visual area (Table 4.4) indicated that mean ISO in V1 was significantly different from V2 and V3. ISO is a complementary NODDI index that models for CSF partial-volume contamination. Since sulci in the brain are filled with CSF and V1 lies along the calcarine sulcus, it is expected that voxels in V1 to have higher levels of CSF contamination.

Repeated measures ANOVA tests (session: pre-, mid- and, post-training) did not reveal any effects on mean ICVF ($F(2, 4) = 0.602, p = 0.591$), mean ODI ($F(2, 4) = 1.117, p = 0.412$), and mean ISO ($F(2, 4) = 6.239, p = 0.059$) at the white matter tract ROI. Descriptive plots can be seen in Figure 4.9.

4.4 Intermediate Discussion

Here, we investigated VPL-induced microstructural changes in the early visual cortex. We computed NODDI indices in the superficial cortical ROIs at the training and control locations to explore neuroplasticity in the local cortical circuitry. Furthermore, we isolated the white matter tract connecting the training location and the homotopic control location in the primary visual cortices of each hemisphere. We analyzed the NODDI indices in this white matter tract ROI to examine training-related changes in the interhemispheric connections.

We did not find any changes in NODDI indices that indicate neuroplasticity in the superficial cortical ROIs. In the gray matter, ICVF and ODI represent

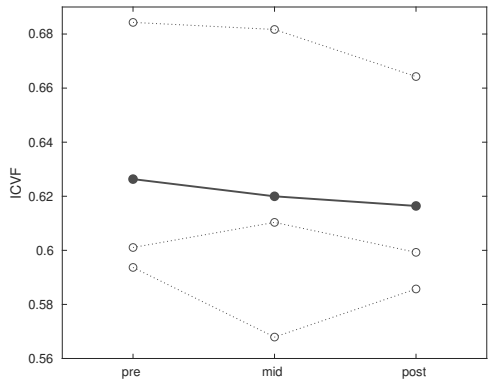

(a) ICVF

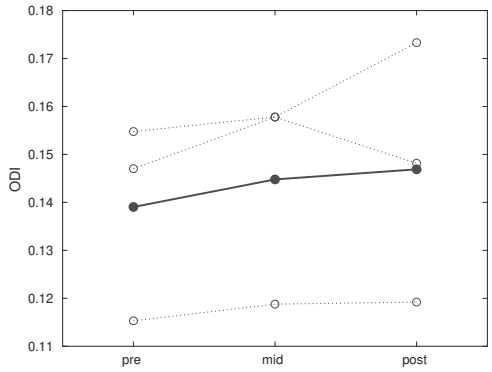

(b) ODI

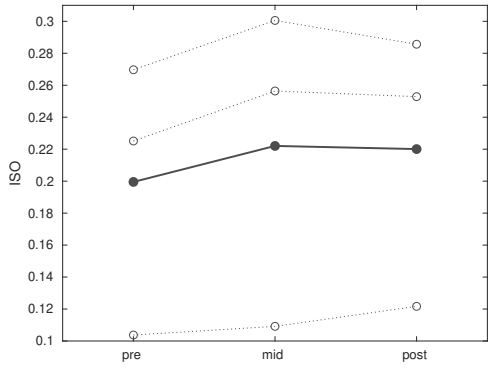

(c) ISO

Figure 4.9: Mean ICVF (a), mean ODI (b), and mean ISO (c) at the white matter tract ROI. The dots show the mean values across subjects, and the rings are individual mean for each subject.

the characteristics of cellular processes that form the neuropil: dendrites and unmyelinated axons. Therefore, changes in horizontal axonal projections and dendritic arborization are expected to be captured by these indices. Previously, axonal plasticity at the trained location in V1 is was reported in monkeys trained with contrast detection task [22]. Similarly, performance improvement in bisection discrimination task was hypothesized to be underpinned by modulation of horizontal connections at the trained location [12]. In contrast, we did not observe any significant difference in mean ICVF or mean ODI of superficial ROIs between sessions and locations.

Consistent with our findings in the superficial ROIs, the white matter tract ROI did not show any change in NODDI indices during training. White matter plasticity has a complementary function to cortical plasticity. Since we did not find any change in cortical microstructure of the superficial V1 ROIs at the training and homotopic control location, we did not expect microstructural alteration of the white matter track that connects these cortical regions.

In sum, we did not find any VPL-induced changes in the microstructure of early visual areas V1, V2, and V3 that would indicate experience-dependent plasticity. However, there might be subtle changes we were not able to detect due to the small sample size in our study.

Chapter 5

General Discussion

In this thesis, we investigated experience-dependent neuroplasticity over the course of perceptual learning of bisection discrimination task. We used model-based MRI methods to examine functional and structural changes in the early visual cortex. Specifically, we used pRF analysis to assess how functional architecture of the visual cortex was affected by perceptual learning. We used NODDI to study potential microstructural changes both in the visual cortex and in the interhemispheric connections between the visual cortices. We did not find any training-related changes indicative of experience-dependent neuroplasticity in the early visual cortex.

The results of pRF analysis presented in Chapter 3 show that pRF size in the early visual areas did not change in response to training. Consistent with our result, it was previously shown that receptive field size in monkey V1 were unaffected by training with bisection discrimination task [12]. Instead of basic receptive field properties, it was suggested that performance on bisection discrimination task depends on contextual tuning of V1 neurons. Contextual tuning arises from interactions between neurons with non-overlapping adjacent receptive fields through long-range horizontal connections and allows the neurons to use information from beyond their classical receptive field. It was proposed that perceptual learning of bisection discrimination task is underpinned by dynamic

modulation of contextual tuning of V1 neurons under top-down control [12] [13]. pRF method as we implemented in this study can not detect this kind of modulatory effect since it was only present during task performance. Moreover, it is not clear how changes in contextual tuning of individual neurons would affect pRF estimates which reflect combined receptive field of the neural population in a given voxel.

In Chapter 3, we investigated the training-related changes to tissue microstructure in the early visual cortex. NODDI analysis of the cortical microstructure presents the opportunity to capture changes to long-range horizontal connections, the anatomical substrate of contextual tuning. We did not observe any change in ICVF or ODI in cortical regions corresponding to trained location. In contrast to a previous study reporting axonal plasticity in response to training with contrast discrimination task [22], our results suggest no change to axonal projections. We also examined microstructural plasticity in the white matter track connecting the training location and homotopic control location in V1 to examine interhemispheric interactions. This analysis did not reveal any training related changes as expected given the complementary role of white matter plasticity.

There is an ongoing debate concerning the extent of neuroplasticity in the adult early visual cortex [53]. While there is consensus that adult visual experience is shaped by the interplay between plasticity and stability, which side the brain favors is the subject of debate. Plasticity provides adaptability to changing environmental conditions throughout our lives. However, stability is also required for an optimized perceptual experience. It is argued that the balance between plasticity and stability is determined by the cost of "coding catastrophe" [54]. When neural code is changed in any level of visual processing hierarchy, the downstream levels must update their interpretation of the neural code for reliable visual perception. Accordingly, the cost is lower when plastic changes occur in higher-level areas instead of the early visual cortex since there are fewer downstream areas that interpret the changed neural code. In a similar vein, the selective reweighting model of perceptual learning supports stability in the early visual cortex and plasticity in higher-levels of visual processing. As explained in the introduction, this model asserts that performance improvement is underpinned by optimized

readout from early sensory representations which remain stable [5, 6]. The lack of training-related changes in the early visual cortex can be seen as in accordance with such notion of experience-dependent neuroplasticity in the visual cortex. Nevertheless, the results of our study are inconclusive due to limitations which will be discussed next.

The primary limitation to this study is the small sample size. As discussed earlier, stability is an important part of normal visual function. Thus the plastic changes in response to training are expected to be subtle in contrast to large-scale changes such as reorganization of the visual cortex as a result of sensory impairment. When combined with the subtlety of changes in the short term experience-dependent plasticity, the small sample size might prevent statistically significant results to be obtained. Unfortunately, it was not possible to recruit more participants due to the global COVID-19 pandemic at the time of study. Moreover, the already small sample size was further scaled down in some cases due to missing data or noneligible analysis results. Although subject exclusion from analysis is not uncommon in research, the combination of longitudinal study design and multimodal MRI approach increases the likelihood of exclusion. For example, we were able to study white matter plasticity in three participants out of the six that took part in the study since the rest were excluded from the analysis pipeline due to various reasons. Increased likelihood of exclusion and discontinuation constitutes a caveat for determining the optimal sample size in similar research.

Another important limitation is the restriction of analysis to the early visual cortex. The current understanding of VPL, as emphasized in the introduction, favors that it involves changes at multiple levels of the visual hierarchy. In order to get a comprehensive understanding of VPL, it is important to treat the visual cortex as a whole instead of focusing on a specific processing level. Accordingly, the main purpose of the study was to investigate VPL-induced plasticity in the visual cortex. However, we were not able to identify high-level visual areas consistently in all participants which led us to restrict our analysis to early visual areas V1, V2, and V3. Therefore, the training-related changes that potentially took place in high-level visual areas were unexplored. The factors that might

have prevented successful delineation of high-level visual areas were discussed in Chapter 3. In light of these considerations, further optimization of both the functional imaging protocol and the stimulus presentation protocol is needed.

In addition to these limitations, the unexpected behavioral effect observed in the training complicates the interpretation of the results. Although not statistically significant, perceptual thresholds at the trained location initially decreased with training but returned to pre-training values by the end of training. In other words, the performance improvement diminished with ongoing training. This is contradicting the literature where performance improvement in VPL is shown to be persistent. The training protocol used in our study consisted of eight sessions run on separate days. While there is no standardized protocol for behavioral training in the VPL literature, similar training intervals are commonly used. A distinguishing aspect of our experimental timeline is the intensity of neuroimaging sessions. The participants attended six MRI sessions each lasting about a period of 1.5 hour. Moreover, the threshold measurements were conducted on the same day after MRI sessions in an attempt to shorten the duration of experiment. Such time-consuming MRI sessions might deplete the motivation of participants which in turn might reflect itself as decrease in task performance.

Although VPL does not require external reinforcement, both feedback [55] and reward [56] have been shown to accelerate the rate of learning and enhance performance improvement. By utilizing this facilitatory effect of external reinforcement, it might be possible to observe faster and stronger learning effects and shorten the experimental duration. We did not benefit from external reinforcement. The monetary reward provided in our experiment did not serve as an external reinforcement since it did not vary with performance. Moreover, no feedback was given during behavioral training. Considering the inconsistent learning effect we observed, it might be favorable to provide both feedback and reward in such a long experimental timeline.

In conclusion, we report no experience-dependent plasticity in early visual cortex following training in bisection discrimination task. However, the small sample

size renders the results inconclusive. Moreover, we cannot rule out the possibility that the lack of plastic changes was due to the failure of behavioral training since we did not observe a significant improvement in performance with training. Nevertheless, the model-based neuroimaging approach we employed here offers a unique opportunity for fine-scale examination of functional and structural changes in the visual cortex and has the potential to provide a more in-depth understanding of VPL-induced plasticity.

As explained previously in Chapter 2, the work presented in this thesis is part of an extensive research project that investigates experience-dependent plasticity in response to VPL by combining task-based fMRI, resting-state fMRI, pRF analysis, tractography and NODDI analysis together. Although we focused on the plasticity in the visual cortex here, it would be possible to conduct a whole-brain multimodal investigation of VPL-induced plasticity within the scope of this project. This provides the opportunity to simultaneously examine all proposed loci of plasticity: early visual areas, higher visual areas, decision making regions, and connectivity between visual cortex and decision making regions. Despite requiring further optimization, we were able to build the analysis pipeline that would allow the integration of findings from multiple neuroimaging modalities. This would allow combining findings obtained from different neuroimaging techniques to overcome the limitations of each technique and to understand brain dynamics underlying VPL with greater detail. In the future, it is necessary to increase the sample size to reveal the full potential of the proposed analysis pipeline.

Bibliography

[1] A. Karni and D. Sagi, "Where practice makes perfect in texture discrimination: Evidence for primary visual cortex plasticity," *Proceedings of the National Academy of Sciences of the United States of America*, vol. 88, pp. 4966–4970, jun 1991.

[2] D. Sagi, "Perceptual learning in Vision Research," *Vision Research*, vol. 51, pp. 1552–1566, jul 2011.

[3] M. Ahissar and S. Hochstein, "Task difficulty and the specificity of perceptual learning," *Nature*, vol. 387, pp. 401–406, may 1997.

[4] M. Ahissar and S. Hochstein, "The reverse hierarchy theory of visual perceptual learning," *Trends in Cognitive Sciences*, vol. 8, pp. 457–464, oct 2004.

[5] B. A. Dosher and Z. L. Lu, "Perceptual learning reflects external noise filtering and internal noise reduction through channel reweighting," *Proceedings of the National Academy of Sciences of the United States of America*, vol. 95, pp. 13988–13993, nov 1998.

[6] A. A. Petrov, B. A. Dosher, and Z. L. Lu, "The dynamics of perceptual learning: An incremental reweighting model," *Psychological Review*, vol. 112, pp. 715–743, oct 2005.

[7] L. Q. Xiao, J. Y. Zhang, R. Wang, S. A. Klein, D. M. Levi, and C. Yu, "Complete Transfer of Perceptual Learning across Retinal Locations Enabled by Double Training," *Current Biology*, vol. 18, pp. 1922–1926, dec 2008.

[8] A. Schoups, R. Vogels, N. Qian, and G. Orban, "Practising orientation identification improves orientation coding in V1 neurons," *Nature*, vol. 412, pp. 549–553, aug 2001.

[9] G. M. Ghose, T. Yang, and J. H. Maunsell, "Physiological correlates of perceptual learning in monkey V1 and V2," *Journal of Neurophysiology*, vol. 87, no. 4, pp. 1867–1888, 2002.

[10] T. Yang and J. H. Maunsell, "The Effect of Perceptual Learning on Neuronal Responses in Monkey Visual Area V4," *Journal of Neuroscience*, vol. 24, pp. 1617–1626, feb 2004.

[11] T. Hua, P. Bao, C. B. Huang, Z. Wang, J. Xu, Y. Zhou, and Z. L. Lu, "Perceptual Learning Improves Contrast Sensitivity of V1 Neurons in Cats," *Current Biology*, vol. 20, pp. 887–894, may 2010.

[12] R. E. Crist, W. Li, and C. D. Gilbert, "Learning to see: Experience and attention in primary visual cortex," *Nature Neuroscience*, vol. 4, no. 5, pp. 519–525, 2001.

[13] W. Li, V. Piëch, and C. D. Gilbert, "Perceptual learning and top-down influences in primary visual cortex," *Nature Neuroscience*, vol. 7, pp. 651–657, jun 2004.

[14] C. T. Law and J. I. Gold, "Neural correlates of perceptual learning in a sensory-motor, but not a sensory, cortical area," *Nature Neuroscience*, vol. 11, pp. 505–513, apr 2008.

[15] S. Schwartz, P. Maquet, and C. Frith, "Neural correlates of perceptual learning: A functional MRI study of visual texture discrimination," *Proceedings of the National Academy of Sciences of the United States of America*, vol. 99, pp. 17137–17142, dec 2002.

[16] C. S. Furmanski, D. Schluppeck, and S. A. Engel, "Learning strengthens the response of primary visual cortex to simple patterns," *Current Biology*, vol. 14, pp. 573–578, apr 2004.

[17] Y. Yotsumoto, T. Watanabe, and Y. Sasaki, "Different Dynamics of Performance and Brain Activation in the Time Course of Perceptual Learning," *Neuron*, vol. 57, pp. 827–833, mar 2008.

[18] J. D. Cohen, N. Daw, B. Engelhardt, U. Hasson, K. Li, Y. Niv, K. A. Norman, J. Pillow, P. J. Ramadge, N. B. Turk-Browne, and T. L. Willke, "Computational approaches to fMRI analysis," feb 2017.

[19] T. Kahnt, M. Grueschow, O. Speck, and J. D. Haynes, "Perceptual Learning and Decision-Making in Human Medial Frontal Cortex," *Neuron*, vol. 70, pp. 549–559, may 2011.

[20] K. Shibata, T. Watanabe, Y. Sasaki, and M. Kawato, "Perceptual learning incepted by decoded fMRI neurofeedback without stimulus presentation," *Science*, vol. 334, pp. 1413–1415, dec 2011.

[21] N. Chen, T. Bi, T. Zhou, S. Li, Z. Liu, and F. Fang, "Sharpened cortical tuning and enhanced cortico-cortical communication contribute to the long-term neural mechanisms of visual motion perceptual learning," *NeuroImage*, vol. 115, pp. 17–29, jul 2015.

[22] T. Van Kerkoerle, S. A. Marik, S. M. Z. A. Borgloh, and C. D. Gilbert, "Axonal plasticity associated with perceptual learning in adult macaque primary visual cortex," *Proceedings of the National Academy of Sciences of the United States of America*, vol. 115, pp. 10464–10469, oct 2018.

[23] H. Yamahachi, S. A. Marik, J. N. McManus, W. Denk, and C. D. Gilbert, "Rapid Axonal Sprouting and Pruning Accompany Functional Reorganization in Primary Visual Cortex," *Neuron*, vol. 64, pp. 719–729, dec 2009.

[24] Y. Wang, W. Wu, X. Zhang, X. Hu, Y. Li, S. Lou, X. Ma, X. An, H. Liu, J. Peng, D. Ma, Y. Zhou, and Y. Yang, "A Mouse Model of Visual Perceptual Learning Reveals Alterations in Neuronal Coding and Dendritic Spine Density in the Visual Cortex," *Frontiers in Behavioral Neuroscience*, vol. 10, p. 42, mar 2016.

[25] D. W. Kang, D. Kim, L. H. Chang, Y. H. Kim, E. Takahashi, M. S. Cain, T. Watanabe, and Y. Sasaki, "Structural and Functional Connectivity Changes beyond Visual Cortex in a Later Phase of Visual Perceptual Learning," *Scientific Reports*, vol. 8, p. 5186, dec 2018.

[26] P. E. Jeter, B. A. Dosher, S. H. Liu, and Z. L. Lu, "Specificity of perceptual learning increases with increased training," *Vision Research*, vol. 50, pp. 1928–1940, sep 2010.

[27] T. Watanabe, J. E. Naánñez, S. Koyama, I. Mukai, J. Liederman, and Y. Sasaki, "Greater plasticity in lower-level than higher-level visual motion processing in a passive perceptual learning task," *Nature Neuroscience*, vol. 5, pp. 1003–1009, sep 2002.

[28] T. Watanabe and Y. Sasaki, "Perceptual Learning: Toward a Comprehensive Theory," *Annual Review of Psychology*, vol. 66, pp. 197–221, jan 2015.

[29] K. Shibata, Y. Sasaki, M. Kawato, and T. Watanabe, "Neuroimaging evidence for 2 types of plasticity in association with visual perceptual learning," 2016.

[30] A. Karni, D. Tanne, B. S. Rubenstein, J. J. Askenasy, and D. Sagi, "Dependence on REM sleep of overnight improvement of a perceptual skill," *Science*, vol. 265, pp. 679–682, jul 1994.

[31] M. P. Walker, R. Stickgold, F. A. Jolesz, and S.-S. Yoo, "The Functional Anatomy of Sleep-dependent Visual Skill Learning," *Cerebral Cortex*, vol. 15, no. 11, pp. 1666–1675, 2005.

[32] M. F. Glasser, S. M. Smith, D. S. Marcus, J. L. Andersson, E. J. Auerbach, T. E. Behrens, T. S. Coalson, M. P. Harms, M. Jenkinson, S. Moeller, E. C. Robinson, S. N. Sotiropoulos, J. Xu, E. Yacoub, K. Ugurbil, and D. C. Van Essen, "The Human Connectome Project's neuroimaging approach," sep 2016.

[33] R. Rajimehr and R. B. Tootell, "Does retinotopy influence cortical folding in primate visual cortex?," *Journal of Neuroscience*, vol. 29, pp. 11149–11152, sep 2009.

[34] S. O. Dumoulin and B. A. Wandell, "Population receptive field estimates in human visual cortex," *NeuroImage*, vol. 39, pp. 647–660, jan 2008.

[35] B. M. Harvey and S. O. Dumoulin, "The Relationship between Cortical Magnification Factor and Population Receptive Field Size in Human Visual Cortex: Constancies in Cortical Architecture," 2011.

[36] I. Alvarez, B. de Haas, C. A. Clark, G. Rees, and D. S. Schwarzkopf, "Comparing different stimulus configurations for population receptive field mapping in human fMRI," *Frontiers in Human Neuroscience*, vol. 9, p. 96, feb 2015.

[37] J. A. van Dijk, B. de Haas, C. Moutsiana, and D. S. Schwarzkopf, "Intersession reliability of population receptive field estimates," *NeuroImage*, vol. 143, pp. 293–303, dec 2016.

[38] B. De Haas, D. S. Schwarzkopf, E. J. Anderson, and G. Rees, "Perceptual load affects spatial tuning of neuronal populations in human early visual cortex," jan 2014.

[39] D. W. Bressler and M. A. Silver, "Spatial attention improves reliability of fMRI retinotopic mapping signals in occipital and parietal cortex," *NeuroImage*, vol. 53, pp. 526–533, nov 2010.

[40] S. Mori and J. Zhang, "Principles of Diffusion Tensor Imaging and Its Applications to Basic Neuroscience Research," sep 2006.

[41] B. Jeurissen, A. Leemans, J.-D. Tournier, D. K. Jones, and J. Sijbers, "Investigating the prevalence of complex fiber configurations in white matter tissue with diffusion magnetic resonance imaging," *Human Brain Mapping*, vol. 34, pp. 2747–2766, nov 2013.

[42] J. D. Tournier, F. Calamante, and A. Connelly, "Robust determination of the fibre orientation distribution in diffusion MRI: Non-negativity constrained super-resolved spherical deconvolution," *NeuroImage*, vol. 35, pp. 1459–1472, may 2007.

[43] S. Farquharson, J.-D. Tournier, F. Calamante, G. Fabinyi, M. Schneider-Kolsky, G. D. Jackson, and A. Connelly, "White matter fiber tractography: why we need to move beyond DTI," *Journal of Neurosurgery*, 2013.

[44] C. Beaulieu, "The Biological Basis of Diffusion Anisotropy," in *Diffusion MRI: From Quantitative Measurement to In vivo Neuroanatomy: Second Edition*, 2013.

[45] H. Zhang, T. Schneider, C. A. Wheeler-Kingshott, and D. C. Alexander, "NODDI: Practical in vivo neurite orientation dispersion and density imaging of the human brain," *NeuroImage*, 2012.

[46] C. Andica, K. Kamagata, T. Hayashi, A. Hagiwara, W. Uchida, Y. Saito, K. Kamiya, S. Fujita, T. Akashi, A. Wada, M. Abe, H. Kusahara, M. Hori, and S. Aoki, "Scan–rescan and inter-vendor reproducibility of neurite orientation dispersion and density imaging metrics," *Neuroradiology*, vol. 62, pp. 483–494, apr 2020.

[47] A. W. Chung, K. K. Seunarine, and C. A. Clark, "NODDI reproducibility and variability with magnetic field strength: A comparison between 1.5 T and 3 T," *Human Brain Mapping*, vol. 37, pp. 4550–4565, dec 2016.

[48] E. Wenger, C. Brozzoli, U. Lindenberger, and M. Lövdén, "Expansion and Renormalization of Human Brain Structure During Skill Acquisition," dec 2017.

[49] C. Sampaio-Baptista and H. Johansen-Berg, "White Matter Plasticity in the Adult Brain," dec 2017.

[50] M. Froeling, C. M. Tax, S. B. Vos, P. R. Luijten, and A. Leemans, ""MASSIVE" brain dataset: Multiple acquisitions for standardization of structural imaging validation and evaluation," *Magnetic Resonance in Medicine*, vol. 77, no. 5, pp. 1797–1809, 2017.

[51] A. Leemans, B. Jeurissen, J. Sijbers, and D. K. Jones, "ExploreDTI: a graphical toolbox for processing, analyzing, and visualizing diffusion MR data," in *Proceedings of the International Society for Magnetic Resonance in Medicine*, vol. 17, p. 3537, 2009.

[52] A. Daducci, E. J. Canales-Rodríguez, H. Zhang, T. B. Dyrby, D. C. Alexander, and J. P. Thiran, "Accelerated Microstructure Imaging via Convex Optimization (AMICO) from diffusion MRI data," *NeuroImage*, vol. 105, pp. 32–44, jan 2015.

[53] B. A. Wandell and S. M. Smirnakis, "Plasticity and stability of visual field maps in adult primary visual cortex," dec 2009.

[54] K. V. Haak, A. B. Morland, and S. A. Engel, "Plasticity, and its limits, in adult human primary visual cortex," *Multisensory Research*, vol. 28, pp. 297–307, apr 2015.

[55] M. H. Herzog and M. Fahle, "The role of feedback in learning a vernier discrimination task," *Vision Research*, vol. 37, pp. 2133–2141, aug 1997.

[56] P. Zhang, F. Hou, F. F. Yan, J. Xi, B. R. Lin, J. Zhao, J. Yang, G. Chen, M. Y. Zhang, Q. He, B. A. Dosher, Z. L. Lu, and C. B. Huang, "High reward enhances perceptual learning," *Journal of Vision*, vol. 18, pp. 1–21, aug 2018.